INFLUENCE OF CONCRETE STRENGTH AND CONFINEMENT METHOD ON AXIAL COMPRESSIVE BEHAVIOR OF FRP CONFINED HIGH- AND ULTRA HIGH- STRENGTH CONCRETE

Thomas Vincent[1] and Togay Ozbakkaloglu[2]

[1] PhD Candidate, School of Civil, Environmental and Mining Engineering, University of Adelaide, Australia. Email

[2] (Corresponding author) Senior Lecturer, School of Civil, Environmental and Mining Engineering, University of Adelaide, Australia. Tel : + 618 8303 6477; Fax : +618 8303 4359; Email: togay.ozbakkaloglu@adelaide.edu.au

ABSTRACT

This paper presents an experimental investigation on the effect of concrete compressive strength and confinement method on confined high and ultra high-strength concrete (HSC and UHSC) specimens. A total of 55 fiber reinforced polymer (FRP) confined concrete specimens were tested under monotonic axial compression. All specimens were cylinders with 152 mm diameter and 305 mm height and confined by carbon FRP (CFRP). Three different concrete mixes were examined, with average compressive strengths of 35, 65 and 100 MPa. The effect of the confinement method was also examined with FRP-wrapped specimens compared to FRP tube-encased specimens. Axial and lateral behavior was recorded to observe the axial stress-strain relationship and lateral strain behavior for concentric compression. Ultimate axial and lateral conditions are tabulated and the complete stress-strain curves have been provided. The experimental results presented in this paper provide a performance comparison between FRP-confined conventional normal-strength concrete (NSC) and the lesser understood area of FRP-confined HSC and UHSC. The results of this experimental study clearly indicate that above a certain confinement threshold, FRP-confined HSC and UHSC exhibits highly ductile behavior, however for the same normalized confinement pressures, axial performance of FRP-confined concrete reduces as concrete strength increases. The results also indicate that ultimate conditions of FRP-wrapped specimens are similar to those confined by FRP tubes, however a

performance difference is evident at the transition region. The performance of 10 existing stress-strain models were assessed against the experimental datasets and the performance of these models discussed. The results of this model assessment revealed the need for further development for stress-strain models developed specifically for FRP-confined HSC or UHSC.

KEYWORDS: FRP-confined concrete; A. Carbon fiber; B. Plastic deformation; B. Strength; D. Mechanical testing

1. INTRODUCTION

It is well established that external confinement of concrete with fiber reinforced polymer (FRP) jackets results in significant improvements of the axial and dilation performance of concrete. A recent comprehensive review study (Ozbakkaloglu et al. [1]) revealed that over 200 experimental studies have been conducted over the last two decades on the compressive behavior of FRP-confined concrete resulting in the developments of over 80 axial stress-strain models (e.g. [2-10]). However, the majority of these studies focused on FRP-confined specimens manufactured with FRP-wrapped jackets, and studies examining the behavior of FRP tube-encased concrete remain limited. The experimental studies on FRP-confined high strength concrete (HSC) have also been limited with many recent studies stating the increased need for further investigations on the behavior of FRP-confined HSC [9, 11-17].

High- and ultra high-strength concrete (HSC and UHSC) are materials that offer significantly better structural engineering properties compared with conventional NSC, and form an attractive alternative to other construction materials. The use of higher strength concretes in construction allows for the reduction in member size which reduces building dead loads and provides a more efficient use of concrete. The use of HSC or UHSC for FRP-confinement is an attractive option due to the efficient combination of two high strength materials forming a high performance member whilst eliminating the inherent brittle nature normally associated with higher strength concretes. The potential benefits of confining HSC or UHSC with FRP have been examined by only a handful of studies which reported on FRP-wrapped HSC [9, 14, 15, 17-22] and only two on FRP tube-encased HSC [16, 23]. It follows, therefore, that experimental investigations into FRP-confined HSC or UHSC, in general, and on FRP tube-encased HSC or UHSC in particular, remain very limited.

This paper reports on an experimental investigation into FRP-confined HSC and UHSC on a total of 55 monotonically loaded circular specimens. 23 of these specimens had an average concrete compressive strength between 55 and 100 MPa and are classified as high-strength concrete (HSC), 21 specimens had concrete strengths greater than 100 MPa and are classified as ultra high-strength concrete (UHSC). In addition to these, 11 NSC specimens were also tested to establish reference values to allow a comparison between NSC and higher strength concrete specimens. 35 of the specimens were manufactured as FRP tube-encased specimens with concrete poured into precast FRP tubes, whereas the remaining 20 specimens were manufactured as FRP-wrapped cylinders. This paper tabulates the ultimate conditions of the test specimens and graphically presents their complete axial stress-strain response. Initially the results of the test program, which was aimed at investigating the influence of concrete strength and confinement method on FRP-confined concrete, are presented. Following this, results of the test program are discussed, where the two aforementioned influences are examined along with other key experimental outcomes. Finally, a model performance assessment is presented where 10 existing stress-strain models are assessed against the test results.

2. TEST PROGRAM

2.1 Details of Specimens

A total of 55 carbon FRP (CFRP) confined cylindrical specimens, all with 152 mm diameter (D) and 305 mm height (H), were manufactured and tested. Three different concrete mixes were used with target compressive strengths of 30, 60 and 90 MPa and labeled as NSC, HSC and UHSC respectively. Plain concrete cylinders with 100 by 200 mm dimensions were tested at selected time intervals to determine the in-place unconfined concrete strength gain. 35 of the specimens were manufactured as FRP tube-encased specimens, where the tubes were prepared using a manual wet lay-up process by wrapping epoxy resin impregnated carbon fiber sheets around precision-cut high-density Styrafoam

templates in the hoop direction. The remaining 20 specimens were FRP-wrapped, prepared using the same manual wet lay-up process, however the epoxy resin impregnated carbon fiber sheets were wrapped directly onto the precast concrete cylinders. The summary of these test specimens is presented in *Table 1*.

The number of FRP layers was selected dependent on concrete strength with higher strength concrete specimens receiving proportionally more layers to ensure adequate confinement. NSC specimens were developed with 1 or 2 layers, HSC specimens with 1 to 4 layers and UHSC with 1 to 6 layers. 3 nominally identical specimens were manufactured and tested for each confinement parameter unless marked otherwise in *Table 1*.

2.2 Material Properties

2.2.1 Concrete

The NSC concrete used in this research was sourced from a local concrete supplier. The HSC and UHSC mixes, on the other hand, were batched and mixed in the laboratory. Both of these mixes consisted of crushed limestone as the coarse aggregate, with a 10 mm nominal maximum diameter. Glenium 27 superplasticiser was added at different amounts to HSC and UHSC mixes to ensure a workable concrete, which resulted in slumps of over 200 mm for both mixes. Control cylinders with 100 by 200 mm dimensions were cast from the NSC, HSC and UHSC mixes and tested in parallel to the FRP-confined specimens to determine compressive strength. The in-place concrete strengths (f'_{co}) reported in *Table 2* were established from the cylinder strengths (f'_c) while allowing for differences in cylinder size and curing conditions of concrete.

2.2.2 FRP

The material properties of the carbon fiber unidirectional sheets used to manufacture the FRP tubes and jackets are shown in *Table 3*. The FRP epoxy adhesive used consisted of two parts, epoxy resin binder (MBrace Saturant) and thixotropic epoxy adhesive (MBrace Laminate Adhesive), which were mixed in the ratio of 3:1. For FRP-wrapped cylinders, a thin layer of epoxy resin was applied to the concrete surface prior to manually wrapping the carbon fiber sheet in the hoop direction. For FRP tube-encased cylinders, the first carbon fiber sheet was wrapped directly onto the cylindrical mold. All fiber sheets were positioned with fibers aligned in the hoop direction with a 100 mm overlap. Specimens with 1 to 3 layers of CFRP were wrapped with 1 continuous sheet with 1 overlap zone, whereas specimens with 4 to 6 layers were wrapped with 2 FRP sheets creating 2 overlap zones of 100 mm each.

2.3 Instrumentation and Testing Procedure

Axial deformations of the specimens were recorded with four linear variable differential transformers (LVDT), which were mounted at the corners between the loading and supporting steel plates of the test machine as shown in *Figure 1*. The recorded deformations were used in the calculation of the average axial strains along the height of the specimens. In addition, the specimens were also instrumented at the mid-height with two unidirectional strain gauges with a gauge length of 20 mm to measure axial strains. During the initial elastic stage, readings from these strain gauges were used to correct the LVDT measurements, where additional displacements due to closure of the gaps in the setup were also recorded by the LVDTs. Transverse strains were measured by three unidirectional strain gauges having a gauge length of 20 mm that were bonded on the FRP jacket outside the overlap region.

To ensure an even loading surface a thin layer of dental stone was applied at the top surface of the concrete cylinder. The load was applied directly on the concrete core through 25 mm thick 150 mm

diameter precision cut steel discs. The specimens were tested under monotonic axial compression using a 5000 kN capacity universal testing machine. During the initial elastic stage of the behavior, the loading was applied with load control at 3 kN per second, whereas displacement control was used at approximately 0.003 mm per second beyond the initial softening until specimen failure. The instrumentation and testing equipment used in this experimental study is shown in *Figure 1*.

Axial compressive tests of the FRP-confined specimens started after the 28-day strength of concrete was attained and continued for approximately 3 weeks. The in-place strengths of the unconfined concrete (f'_{co}) at the time of testing are reported together with the corresponding axial strains (ε_{co}) in *Table 2*. ε_{co} values were not measured directly for all the control specimens but were calculated using the expression given by Tasdemir [24].

2.4 Specimen Designation

The specimens presented in *Table 1* were labeled based on their unconfined concrete strength, confinement method and number of FRP layers. Following these 3 key parameters a number was applied to identify between identical specimens. For example the specimen designation of N-T2-3 relates to a specimen manufactured with NSC and confined with a CFRP tube of 2 layers. The final number, '3', identifies that it is the third one of this group of nominally identical specimens.

3. TEST RESULTS

3.1 Observed failure modes

The failure mode for all specimens reported in *Table 2* was either a continuous rupture of the FRP shell from top to bottom or localized FRP rupture at the mid or top sections. *Figure 2* shows examples of both of these observed failure modes where two types of continuous rupture are presented, namely

ringed rupture and top-half failure. It was found that specimens that failed with localized rupture frequently failed in only the upper regions of the specimen. This failure indicates a common weakness of FRP-confined concrete specimens in their upper regions potentially due to the localized effects of concrete shrinkage as evaporation occurs only at the top surface. This effect is limited only to FRP tube-encased specimens as in these specimens the curing of concrete takes place inside the FRP tube. As illustrated in *Figure 2*, typical shear cone formations were evident in all failed specimens independent of FRP confinement method or rupture type.

3.2 Ultimate condition

The ultimate condition, which consists of the ultimate axial strength (f'_{cu}) recorded at failure of the specimen, corresponding axial strain (ε_{cu}) and FRP hoop rupture strain $(\varepsilon_{h,rup})$, of each FRP-confined specimen is reported in *Table 2,* and the full stress-strain relationships are presented in *Figures 3* and *4*. If the stress-strain relationship contained a descending branch so that the determined ultimate strength (f'_{cu}) was lower than the recorded peak strength (f'_{cc}), then both the ultimate (f'_{cu}) and peak (f'_{cc}) strengths were reported in *Table 2*. If the stress-strain relationship contained an ascending branch so that the ultimate strength (f'_{cu}) was the peak strength (f'_{cc}), this value was reported under f'_{cc} in *Table 2*. The ultimate axial strain of each specimen was calculated by averaging the 4 LVDTs readings at failure. For the majority of the specimens this was an easy task with a clear distinctive ultimate point. For some specimens however, the process of establishing a single ultimate point was not straightforward. For example, as shown in *Figure 5*, a single ultimate point does not exist for the specimens presented. Rather a failure range exists (from point A to B) where the specimen initially shows signs of gradual failure at point A but recovers to undergo further axial deformation before the complete failure of the FRP shell at point B. In some instances of gradual failure it is quite clear that the failure range is rapid and unstable, however for other examples the specimen stabilizes and

performs significantly well after the initial failure point A. This gradual failure was found to vary significantly from specimen to specimen even for identical specimens, and for all specimens that experienced this progressive failure, the failure range has been reported in *Table 2*. In determining strength and strain enhancement ratios (f'_{cc}/f'_{co} and $\varepsilon_{cu}/\varepsilon_{co}$) of the specimens that demonstrated a progressive failure, ε_{cu} and f'_{cc}, in specimens with ascending type of curves, were selected as the final stress and strain values prior to catastrophic failure of the specimen, namely point B. It should be noted that the method used in determining the ultimate condition may significantly influence the ultimate strains. Therefore, it would be beneficial to establish a standardized method for the determination of the ultimate condition to improve the consistency of the strain data obtained from different studies in the future.

The average hoop rupture strain $(\varepsilon_{h,rup\ avg})$ of each specimen is presented in *Table 2*, which was averaged from the readings of three lateral strain gauges that were placed outside the overlap region recorded at the time of hoop rupture. The maximum hoop rupture strain $(\varepsilon_{h,rup\ max})$, obtained from the highest reading strain gauge, is also given in *Table 2*. It is now well understood that the hoop rupture strains recorded in FRP-confined concrete specimens $(\varepsilon_{h,rup})$ are often smaller than the ultimate tensile strain of the fibers (ε_{fu}) reported by the manufacturer [5, 11, 25-27]. The strain reduction factor, k_ε, determined from *Eq. 1* using the average hoop rupture strains ($\varepsilon_{h,rup\ avg}$), was established for each group of identical test specimens and are presented in *Table 2*. To ensure reliability, plots of lateral strain development were examined and unreliable strain gauge readings, due to instrumentation problems or partial strain gauge debonding, were omitted.

$$k_\varepsilon = \frac{\varepsilon_{h,rup}}{\varepsilon_{fu}} \qquad (1)$$

The test results of three specimens were deemed unreliable due to difficulties experienced with either the load application or data acquisition system and are marked in *Table 2*. For specimens H-T4-3 and UH-T5-1 the presence of eccentricity during loading was evident, as can be seen from the stress-strain curves, especially near the transition region, in *Figure 3(f and k)*. Specimen UH-T1-3 experienced instrumentation errors related to recordings of axial strain, as such, only ultimate strength values are supplied in *Table 2*. These specimens were excluded when determining average values of strength enhancement ratios (f'_{cc}/f'_{co}), strain enhancement ratios ($\varepsilon_{cu}/\varepsilon_{co}$) and strain reduction factor (k_ε).

4. ANALYSIS OF TEST RESULTS

It is evident from the axial stress-strain relationships presented in *Figures 3* and *4* that HSC and UHSC can exhibit highly ductile behavior when sufficiently confined by either FRP tubes or wraps. On the other hand, lightly confined specimens with confinement levels below a certain threshold exhibit only minimal gains in strength or ductility. It is also evident from *Figures 3* and *4* that as the concrete strength increases, so does the tendency for a slight loss in compressive strength after the initial peak. For HSC and UHSC specimens that have a high level of FRP confinement this slight loss is only temporary with significant gains in strength and strain capacities following this strength loss as can be seen in *Figures 3(e, k and l)* and *4(h and i)*. However, the same is not true for specimens with inadequate levels of confinement, such as all UH-T1, UH-T1 and UH-T2 specimens that display descending second branches with regions of unpredictable fluctuations between rapid strength loss and strength plateau 3 as illustrated in *Figures 3(c, g and h)*.

Further details on the results reported in *Table 2* and the relationships shown in *Figures 3* and *4* are discussed in the following sections where the influence of the key confinement parameters, namely, amount of confinement, concrete compressive strength and method of confinement are presented.

4.1 Influence of Amount of Confinement

The ultimate conditions, tabulated in *Table 2,* indicate that, as expected, the number of FRP layers significantly influences the strength and strain enhancement ratios. *Figure 6* presents an example of the influence of confinement amount by comparing the axial performance of FRP-wrapped HSC specimens with number of layers ranging from 1 to 4. It can be clearly seen that an increase in the amount of confinement results in an increase in both the ultimate axial strength and strain of FRP-confined HSC. On the other hand, as evident from the k_ε values reported in *Table 2* the number of layers did not have a noticeable influence on k_ε and for a given concrete strength range (i.e. NSC, HSC or UHSC) k_ε remained fairly constant for specimens having different amounts of confinement. For example, UHSC tubed specimens ranging from 1 to 6 layers of FRP recorded average k_ε values that fluctuate between 0.47 and 0.55 with no noticeable influence of confinement amount.

4.2 Influence of Concrete Compressive Strength

The influence of in-place strength of concrete is investigated by comparing the axial performance of FRP-confined specimens manufactured with three different concrete strength ranges (i.e. NSC, HSC and UHSC). To allow for a meaningful comparison between specimens of different concrete compressive strengths, the nominal confinement ratio (f_{lu}/f'_{co}), which is the ratio of maximum confinement pressure (f_{lu}) to the in-place unconfined concrete strength (f'_{co}), must be considered. Assuming a uniform confinement pressure distribution, the maximum confinement pressure (f_{lu}) can be calculated by *Eq. 2*.

$$f_{lu} = \frac{2t_f f_{fu}}{D} = \frac{2t_f E_f \varepsilon_{fu}}{D} \qquad \textit{Eq. 2}$$

However, as stated previously the hoop rupture strains ($\varepsilon_{h,rup}$) reported at ultimate conditions are regularly lower than the ultimate tensile strains of fibers reported by manufacturers (ε_{fu}). To account for

this, the strain reduction factor k_ε, is incorporated to determine the actual lateral confining pressure, ($f_{lu,a}$), as:

$$f_{lu,a} = \frac{2t_f f_{fu} k_\varepsilon}{D} = \frac{2t_f E_f \varepsilon_{h,rup}}{D} \qquad \textit{Eq. 3}$$

To maintain comparable values of nominal confinement ratio (f_{lu}/f'_{co}), the specimens of the present study were designed with FRP layers adjusted relative to concrete strength. For example NSC, HSC and UHSC specimens were allocated one, two and three layers of CFRP, respectively. This same process was then repeated for two, four and six layers for the second group of comparable specimens. It should be noted that due to slight differences between target and test day in-place concrete strengths (f'_{co}) as well as differences in recorded strain reduction factors (k_ε), as influenced by concrete strength, values of actual confinement ratio ($f_{lu,a}/f'_{co}$) differed slightly within each group.

Figure 7 illustrates the influence of the concrete strength on the axial performance of the specimens, separately for wrapped and tube-encased specimens, where normalized axial stress (f_{cc}/f'_{co}) is plotted against normalized axial strain ($\varepsilon_{cc}/\varepsilon_{co}$). It can be seen in *Figure 7* that, in general, an increase in concrete compressive strength (f'_{co}) leads to an overall decrease in both the strength enhancement ratio (f'_{cc}/f'_{co}) and strain enhancement ratio ($\varepsilon_{cc}/\varepsilon_{co}$). It should be noted that the comparison in *Figure 7(a)* illustrates a similar performance level for the NSC specimen N-T1-2 and the HSC specimen H-T2-1; however, this comparable performance can be attributed to H-T2-1 gaining an advantage from a significantly higher $f_{lu,a}/f'_{co}$ ratio.

Figures 8(a) and *8(b)* present a graphical comparison of the influence of concrete strength on the ultimate conditions of the specimens. Only specimens featuring ascending second branches are included in this comparison. In these figures the strength and strain enhancement ratios for all NSC, HSC and UHSC specimens are shown together with the trend lines established for each group of

specimens. It is evident from these figures that the axial strength and strain enhancement ratios of FRP-confined concrete decrease as the strength of concrete increases.

Table 4 presents the average hoop strain reduction factors (k_ε) and corresponding standard deviation (*S.D.*) from all specimens for each concrete strength range and both types of confinement methods. It is clear from the results reported in this table that concrete compressive strength influences the mean k_ε, with NSC, HSC and UHSC specimens experiencing average strain reduction factors of 0.747, 0.651 and 0.519, respectively. This trend indicates that an increase in concrete compressive strength (f'_{co}) causes a decrease in strain reduction factor (k_ε). This influence was first reported in Ozbakkaloglu and Akin [17] and it can be attributed to the increased concrete brittleness with increasing concrete strength, which alters the concrete crack patterns from heterogenic microcracks to localized macrocracks.

It should be noted that the strain reduction factors (k_ε) given in *Table 4,* are in general lower than those reported in previous studies (e.g. [28]). Noting that the majority of the specimens of the present study were HSC or UHSC, this difference can be explained by the aforementioned influence of the concrete strength (f'_{co}) on k_ε. It should also be noted that the most damaged sections of the specimens not always corresponded to the sections that were instrumented for the measurement of the FRP hoop strains. This too might have contributed to the slightly lower k_ε values reported in this study.

4.3 Influence of Confinement Method

Figures 3 and *4* present axial stress-strain relationships of FRP tube-encased and FRP-wrapped specimens, respectively. A comparison of these two figures reveals similar axial performance levels between FRP tube-encased and FRP-wrapped specimens with otherwise identical parameters. It can be

seen that specimens prepared with either confinement method behave similarly in terms of the trend of the second branch and ultimate conditions. However, when a comparison is made of the stress-strain behavior near the location of the unconfined concrete peak stress a noticeable difference can be seen. At this stage of the stress-strain curve the expanding concrete activates the FRP-shell and causes a gradual transition between the initial ascending branch and second branch of the stress-strain curve. It is evident in this comparison that FRP tube-encased specimens frequently experience a shorter transition zone. This trend is shown in *Figure 9* where the activation of the FRP shell occurs earlier in the ascending branch for the wrap confined specimens leading to a longer and more gradual transition into the ascending second branch. The results of this comparison indicate a delayed activation of the confining FRP shell for specimens constructed with FRP tubes. This delayed activation trend indicates that the process of concrete shrinkage during curing, which is isolated to only FRP tube-encased specimens, affects the transition zone behavior of FRP-confined concrete. It should be noted that the FRP tube-encased specimens of the present study were kept in a fog room during their curing period. Therefore, it was highly unlikely that the concrete in these FRP tubes had developed significant shrinkage. FRP tube-encased specimens that are exposed to different curing conditions may develop different shrinkage behavior, which could affect their dilation behavior under axial compression and in turn may result in more noticeable difference in stress-strain behavior compared to their FRP-wrapped counterparts.

It can be seen in *Table 4* that, for a given strength range, the method of confinement only slightly influences both the mean and standard deviation of the average hoop strain reduction factor (k_ε). Therefore, the results of the present study indicate that confinement method does not influence k_ε for a given concrete strength range.

A graphical comparison of the influence of confinement method on the ultimate conditions of FRP-confined concrete is presented in *Figures 10* and *11*. The figures show, respectively, the strength and strain enhancement ratios (f'_{cc}/f'_{co} and $\varepsilon_{cc}/\varepsilon_{co}$), that are plotted against actual confinement ratio ($f_{lu,a}/f'_{co}$) for the NSC and HSC specimens separately. The comparison for the UHSC specimens was omitted due to limited test data for FRP-wrapped specimens. It is evident from the trend lines shown in the figures that for both strength and strain enhancement, wrapped and tube-encased specimens demonstrate quite similar behavior, with near identical trend lines.

5. COMPARISON OF TEST RESULTS WITH PREDICTIONS OF EXISTING STRESS-STRAIN MODELS

The experimental results of the present study were compared with 10 models proposed for predicting the axial strength and strain enhancement ratios of FRP-confined concrete (f'_{cc}/f'_{co} and $\varepsilon_{cc}/\varepsilon_{co}$). These 10 models, presented in *Table 5*, were selected from a recent comprehensive model review study reported in Ozbakkaloglu et al. [1], where over 80 models were reviewed and assessed. The models included in this paper were chosen based three main factors. Foremost, models were selected for their ability to predict both the ultimate strength and strain. The second criterion was model format, where models were considered only if originally presented in simple close-form equation format. Finally, models were selected with proven good performance for FRP-confined NSC as recently assessed in Ozbakkaloglu et al. [1]. Because these models were given to predict the ultimate condition of FRP-confined concretes exhibiting ascending type of second branches, only the specimens that demonstrated ascending type post-peak responses were included in this comparison.

Three statistical indicators were used to assess the performance of the models: the mean square error (*MSE*), the average absolute error (*AAE*) and the linear trend slope (*LTS)*. The mean square error (*MSE*)

and the average absolute error (*AAE*), defined by *Eq. 4* and *Eq. 5* respectively, were used as the statistical indicators of modeling accuracy where lower values indicated better model performance. The linear trend slope (*LTS*), determined by a regression analysis, was used to describe the associated average overestimation or underestimation of the model, where an overestimation is represented by a linear trend slope greater than 1. *Table 6* presents the summary of the model assessment.

$$MSE = \sum_{i=1}^{n} \frac{(\mathrm{mod}_i - \exp_i)^2}{N} \qquad \textit{Eq. 4}$$

$$AAE = \frac{\sum_{i=1}^{n} \left| \frac{\mathrm{mod}_i - \exp_i}{\exp_i} \right|}{N} \qquad \textit{Eq. 5}$$

The comparison of the experimental results with model predictions is also presented graphically in *Figures 12* and *13,* respectively, for the ultimate strength and strain. It can be seen in this model comparison that majority of the models perform reasonably well in predicting ultimate strength and strain of FRP-confined NSC. However, it is clear that model performances degrade significantly, in both strength and strain predictions, when they are applied to HSC or UHSC specimens. It can be seen in *Table 6* that in general, both statistical indicators of error, MSE and AAE, increase with an increase in concrete compressive strength. This trend is clearly evident for all predictions of strength enhancement (f'_{cc}/f'_{co}), whereas a few exceptions exist for predictions of strain enhancement ($\varepsilon_{cc}/\varepsilon_{co}$) with Benzaid et al. [29], Bisby et al. [6] and Tamuzs et al. [30, 31] recording lower values of AAE with increasing concrete strength. In the assessment presented in *Table 6* it can be seen that most models performed with a high level of error when applied to HSC and UHSC specimens with no current model predicting both ultimate strength and strain of these specimens with an AAE less than 15%. It is clear from this observation that none of the current models provide sufficient accuracy in predicting the ultimate conditions of FRP-confined HSC and UHSC. It can also be seen in *Table 6* that the recorded values of LTS increase with an increase in concrete compressive strength indicating most models have

a tendency to overestimate the ultimate conditions of FRP-confined concrete. The above observations point to the need for development of stress-strain models that are applicable to HSC and UHSC.

6. CONCLUSIONS

This paper has reported the results of an experimental investigation into the influence of concrete compressive strength and confinement method on the compressive behavior of FRP-confined high- and ultra high-strength concrete. Based on the observations reported and discussed in this paper, the following conclusions can be drawn:

1. When sufficiently confined, FRP-confined high- and ultra high-strength concrete can exhibit highly ductile compressive behavior. However if the HSC or UHSC is inadequately confined, the axial compressive performance of the FRP tube-encased or FRP-wrapped specimen degrades significantly.
2. For the same actual confinement ratios ($f_{lu,a}/f'_{co}$), strength enhancement (f'_{cc}/f'_{co}) and strain enhancement ratios ($\varepsilon_{cu}/\varepsilon_{co}$) increase as the in-place concrete compressive strength (f'_{co}) decreases.
3. For the confinement levels studied, FRP thickness and confinement method does not significantly affect strain reduction factor k_{ε}, whereas concrete strength has a noticeable influence, and the strain reduction factor decreases with an increase in concrete compressive strength.
4. Within the compressive strength range and confinement levels examined in this study, FRP-wrapped specimens perform similar to FRP tube-encased specimens in terms of both their ultimate axial strengths and ultimate axial strains. A noticeable difference is observed, however, at the transition region between the first and second branch of the stress strain curve, with tube-encased specimens exhibiting a shorter transition region compared to FRP-wrapped ones. This difference may be attributed to shrinkage of concrete inside the FRP tube during curing.

5. The performance of the existing stress-strain models of FRP-confined concrete degrades significantly, in predicting both the ultimate strength and strain, when they are applied to HSC or UHSC. None of the assessed models is able to provide sufficient accuracy in predicting the ultimate conditions of FRP-confined HSC and UHSC, with the majority of them significantly overestimating both the strength and strain enhancement ratios. The result of this assessment indicates a clear need for development of stress-strain models that can accurately predict the compressive behavior of HSC and UHSC.

7. ACKNOWLEDGEMENTS

The authors would like to thank Ms. Staak and Verma and Messrs. Chan, Haw, Miller, Puan and Rohrlach who performed the experimental programme reported in this study as part of their undergraduate thesis.

8. REFERENCES

1. Ozbakkaloglu, T., Lim, J. C., Vincent, T., *FRP-Confined Concrete in Circular Sections: Review and Assessment of Stress-Strain Models.* Eng. Struct., 2012. **http://dx.doi.org/10.1016/j.engstruct.2012.06.010.**
2. Xiao, Y., and Wu, H. , *Compressive behavior of concrete confined by carbon fiber composite jackets.* J. Mater. Civ. Eng., 2000. **12**(2): p. 139 - 146.
3. Harries, K.A., and Kharel, G., *Behavior and modeling of concrete subject to variable confining pressure.* ACI Mater. J., 2002. **99**(2): p. 180 - 189.
4. Karabinis, A.I., and Rousakis, T. C. , *Concrete confined by FRP material: a plasticity approach.* ASCE J. Eng. Struct., 2002. **24**(7): p. 923 - 932.

5. Lam, L., and Teng, J. G., *Design-oriented stress-strain model for FRP-confined concrete.* Constr. Build. Mater., 2003. **17**(6&7): p. 471 - 489.

6. Bisby, L.A., Dent, A. J. S., Green, M. F. , *Comparison of confinement models for fiber-reinforced polymer-wrapped concrete.* ACI Struct. J., 2005. **102**(1): p. 62-72.

7. Ilki, A., Peker, O., Karamuk, E., Demir, C., Kumbasar, N., *FRP retrofit of low and medium strength circular and rectangular reinforced concrete columns.* J. Mater Civ Eng, 2008. **20**(2): p. 169-188.

8. Wang, L.M., and Wu, Y. F. , *Effect of Corner Radius on the Performance of CFRP-Confined Square Concrete Columns: Test.* Eng. Struct., 2008. **30**(2): p. 493 - 505.

9. Xiao, Q., Teng, J. G., and Yu, T. , *Behavior and Modeling of Confined High-Strength Concrete.* ASCE J. Compos. Constr., 2010. **14**(3): p. 249 - 259.

10. Yazici, V., and Hadi, M. N., *Normalized Confinement Stiffness Approach for Modeling FRP-Confined Concrete.* ASCE J. Compos. Constr., 2012. **16**(5): p. 520 - 528.

11. Lam, L., and Teng, J. G., *Ultimate condition of FRP-confined concrete.* ASCE J. Compos. Constr., 2004. **8**(6): p. 539 - 548.

12. Ozbakkaloglu, T., and Saatcioglu, M. , *Seismic behavior of high-strength concrete columns confined by fiber reinforced polymer tubes.* ASCE J. Compos. Constr., 2006. **10**(6): p. 538-549.

13. Ozbakkaloglu, T., Saatcioglu, M., *Seismic Performance of Square High-Strength Concrete Columns in FRP Stay-in-Place Formwork.* ASCE J. Struct. Eng., 2007. **133**(1): p. 44-56.

14. Eid, R., Roy, N., and Paultre, M., *Normal- and High-Strength Concrete Circular Elements Wrapped with FRP Composites.* ASCE J. Compos. Constr., 2009. **13**(2): p. 113-124.

15. Wu, H., Wang, Y., Yu, L. and Li, X., *Experimental and Computational Studies on High-Strength Concrete Circular Columns Confined by Aramid Fiber-Reinforced Polymer Sheets.* ASCE J. Compos. Constr., 2009. **13**(2): p. 125 - 134.

16. Ozbakkaloglu, T., *Axial Compressive Behavior of Square and Rectangular High-Strength Concrete-Filled FRP Tubes.* ASCE J. Compos. Constr., 2012. **DOI: 10.1061/(ASCE)CC.1943-5614.0000321**.

17. Ozbakkaloglu, T., and Akin, E., *Behavior of FRP-confined normal- and high-strength concrete under cyclic axial compression.* ASCE J. Compos. Constr., 2012. **16**(4): p. 451-463.

18. Rousakis, T., *Experimental investigation of concrete cylinders confined by carbon FRP sheets under monotonic and cyclic axial compressive load.*, in *Research Report*. 2001, Chalmers Univ. of Technology: Göteborg, Sweden.

19. Berthet, J.F., Ferrier. E., and Hamelin. P. , *Compressive behavior of concrete externally confined by composite jackets. Part A: experimental study.* Constr. Build. Mater.,, 2005. **19**(3): p. 223 - 232.

20. Mandal, S., Hoskin, A., and Fam, A. , *Influence of concrete strength on confinement effectiveness of fiber-reinforced polymer circular jackets.* ACI Struct. J., 2005. **102**(3): p. 383 - 392.

21. Almusallam, T.H., *Behaviour of normal and high-strength concrete cylinders confined with E-glass/epoxy composite laminates.* Composites Part B: Engineering., 2007. **38**: p. 629 - 639.

22. Cui, C., and Sheikh, A. , *Experimental Study of Normal- and High-Strength Concrete Confined with Fiber-Reinforced Polymers.* ASCE J. Compos. Constr., 2010. **14**(5): p. 553 - 561.

23. Zohrevand, P., and Mirmiran, A., *Behaviour of Ultrahigh-Performance Concrete Confined by Fiber-Reinforced Polymers.* J. Mater. Civ Eng., 2012. **23**(12): p. 1727 - 1734.

24. Tasdemir, M.A., Tasdemir, C., Jefferson, A. D., Lydon, F. D., and Barr, B. I. G. , *Evaluation of strains at peak stresses in concrete: a three-phase composite model approach.* Cem. Concr. Res., 1998. **20**(4): p. 301 - 318.

25. Pessiki, S., Harries, K. A., Kestner, J., Sause, R., and Ricles, J. M. , *The axial behavior of concrete confined with fiber reinforced composite jackets.* ASCE J. Compos. Constr., 2001. **5**(4): p. 237 - 245.

26. Ilki, A., Kumbasar, N., *Compressive behaviour of carbon fiber composite jacketed concrete with circular and non-circular cross sections.* J. of Earthquake Eng., 2003. **7**(3): p. 381-406.

27. Ozbakkaloglu, T., and Oehlers, D. J., *Manufacture and testing of a novel FRP tube confinement system.* Eng. Struct., 2008. **30**: p. 2448 - 2459.

28. Wu, Y.F., Jiang, J.F., *Effective Strain of FRP for Confined Circular Columns.* Composite Structures, 2013. **95**: p. 479-491.

29. Benzaid, R., Mesbah, H., and Chikh, N., *FRP-confined Concrete Cylinders: Axial Compression Experiments and Strength Model.* J. Reinf. Plas. Compos., 2010. **29**(16): p. 2469 - 2488.

30. Tamuzs, V., Tepfers, R., and Sparnins, E. , *Behavior of concrete cylinders confined by carbon composite II: prediction of strength.* Mech. Compos. Mater., 2006. **42**(2): p. 109 - 118.

31. Tamuzs, V., Tepfers., R, Zile, E., and Ladnova, O. , *Behavior of concrete cylinders confined by a carbon composite III: deformability and the ultimate axial strain.* Mech. Compos. Mater., 2006. **42**(4): p. 303 - 314.

32. Jiang, T., and Teng, J. G. *Strengthening of short circular RC columns with FRP jackets: a design proposal.* in *Proc. 3rd Int. Conf. on FRP Composites in Civil Engineering*. 2006. Miami, Florida, USA.

33. Samaan, M., Mirmiran, A., and Shahawy, M. , *Model of concrete confined by fiber composites.* ASCE J. Struct. Eng., 1998. **124**(9): p. 1025 - 1031.

34. Shehata, I.A.E.M., Carneiro, L. A. V., and Shehata, L. C. D., *Strength of short concrete columns confined with CFRP sheets.* Mater. and Struct., 2002. **35**: p. 50 - 58.

35. Teng, J.G., Jiang, T., Lam, L. and Luo, Y., *Refinement of a Design-Oriented Stress-Strain Model for FRP-Confined Concrete.* ASCE J. Compos. Constr., 2009. **13**(4): p. 269 - 278.

36. Wei, Y.Y., and Wu, Y. F., *Unified stress-strain model of concrete for FRP-confined columns.* Construction and Building Materials, 2012. **26**(1): p. 381 - 392.

37. Youssef, M.N., Feng, M. Q., and Mosallam, A. S. , *Stress-strain model for c oncrete confined by FRP composites.* Composites Part B: Engineering., 2007. **38**(5-6): p. 614 - 628.

LIST OF TABLES

Table 1. Details of test specimens

Confinement Type	*D* (mm)	*H* (mm)	Concrete Batch	FRP Layers	Number of Specimens
Tube-encased	152	305	NSC	1	2
				2	3
			HSC	1	3
				2	3
				3	3
				4	3
			UHSC	1	3
				2	3
				3	3
				4	3
				5	3
				6	3
FRP-wrapped	152	305	NSC	1	3
				2	3
			HSC	1	3
				2	3
				3	2
				4	3
			UHSC	4	1
				5	1
				6	1
				Total	55

Table 2. Test results

Group	Specimen	f'_{co} (MPa)	ε_{co} (%)	f'_{cc} (MPa)	f'_{cu} (MPa)	ε_{cu} (%)	$\varepsilon_{h,rup\ avg}$ (%)	$\varepsilon_{h,rup\ max}$ (%)	f'_{cc}/f'_{co}	$\varepsilon_{cu}/\varepsilon_{co}$	k_ε
NSC tube-encased	N-T1-1	37.3	0.21	42.0		0.79	1.20	1.26	1.16	3.54	0.64
	N-T1-2	34.6	0.20	41.6		0.66	0.77	0.86			
	N-T2-1	35.5	0.20	59.1		1.43	1.32	1.49	1.66	7.16	0.84
	N-T2-2	36.3	0.21	60.9		1.53	1.36	1.55			
	N-T2-3	37.3	0.21	60.9		1.45	1.23	1.23			
HSC tube-encased	H-T1-1	59.0	0.26	58.8	45.2	0.72	0.90	0.97	1.01	2.44	0.64
	H-T1-2	59.0	0.26	60.1	39.0	0.56	1.08	1.26			
	H-T1-3	59.0	0.26	57.3	43.3 - 51.6	0.45 - 0.61	1.03	1.07			
	H-T2-1	62.0	0.26	66.8		0.84	1.03	1.26	1.11	3.64	0.72
	H-T2-2	59.0	0.26	65.4		1.05	1.19	1.25			
	H-T2-3	59.0	0.26	68.4		0.95	1.14	1.37			
	H-T3-1	59.0	0.26	79.2		1.24	1.07	1.24	1.36	5.38	0.64
	H-T3-2	65.0	0.27	77.8 - 78.0		1.18 - 1.30	0.77	0.99			
	H-T3-3	59.0	0.26	81.6		1.54	0.92	0.98			
	H-T4-1	59.0	0.26	73.3 - 78.4		0.88 - 1.14	0.92	1.05	1.41	4.83	0.61
	H-T4-2	59.0	0.26	88.0		1.36	0.98	1.06			
	H-T4-3**	59.0	0.26	81.3		1.23	0.62	0.70			
UHSC tube-encased	UH-T1-1	92.0	0.32	97.6	67.6 - 69.5	0.45 - 0.60	0.78	0.94	1.06	1.65	0.47
	UH-T1-2	85.6	0.31	91.0	81.3	0.45	0.68	0.76			
	UH-T1-3**	92.0	0.32	96.7		-	-	-			
	UH-T2-1	93.1	0.33	97.9	68.1 - 88.9	0.44 - 0.75	0.92	1.05	1.11	2.13	0.50
	UH-T2-2	83.1	0.31	95.6	67.1 - 92.9	0.46 - 0.79	0.92	0.97			
	UH-T2-3	80.4	0.30	89.7		0.46	0.50	0.79			
	UH-T3-1	92.7	0.32	101.3	84.8	0.81	0.75	0.85	1.08	2.59	0.53
	UH-T3-2	94.7	0.33	103.4	99.2	0.89	0.86	0.93			
	UH-T3-3	90.1	0.32	96.0	86.7	0.82	0.84	0.96			
	UH-T4-1	97.5	0.33	107.2		1.01	0.97	1.15	1.08	2.91	0.55
	UH-T4-2	93.0	0.33	97.9	95.9	0.92	0.71	0.72			
	UH-T4-3*	100.0	0.34	107.9	98.9	0.96	0.88	1.10			
	UH-T5-1**	87.0	0.31	110.8	107.8	0.83	0.69	0.70	1.13	3.03	0.52
	UH-T5-2	102.5	0.34	119.2		1.06	0.87	0.89			
	UH-T5-3	102.5	0.34	112.8		1.01	0.74	0.81			
	UH-T6-1	102.5	0.34	121.4 - 131.1		0.99 - 1.27	0.89	1.00	1.26	3.53	0.50
	UH-T6-2*	96.0	0.33	124.2		1.16	0.78	0.84			
	UH-T6-3	93.0	0.33	104.3 - 112.1		0.59 - 1.09	0.66	0.81			
NSC FRP-wrapped	N-W1-1	35.5	0.20	44.0		0.77	1.20	1.29	1.23	3.95	0.73
	N-W1-2	35.5	0.20	43.9		0.82	1.10	1.31			
	N-W1-3	35.5	0.20	43.1		0.82	1.10	1.10			
	N-W2-1	38.0	0.21	63.5		1.51	1.17	1.17	1.68	7.10	0.74
	N-W2-2	38.0	0.21	66.1		1.65	1.17	1.42			
	N-W2-3	36.1	0.20	58.6		1.27	1.11	1.18			
HSC FRP-wrapped	H-W1-1	64.5	0.27	65.6	46.7	0.59	0.93	1.00	1.05	2.23	0.58
	H-W1-2	64.5	0.27	68.7	48.6	0.57	0.81	0.95			
	H-W1-3	62.9	0.27	66.3	50.4	0.65	0.98	1.11			
	H-W2-1	64.5	0.27	72.3		0.93	1.25	1.29	1.09	3.05	0.70
	H-W2-2	62.4	0.27	68.4		0.71	0.94	0.96			
	H-W2-3	64.2	0.27	68.2		0.82	1.08	1.22			
	H-W3-1	64.5	0.27	85.9		1.19	1.07	1.24	1.29	4.05	0.67
	H-W3-2	64.5	0.27	80.3		1.00	1.01	1.20			
	H-W4-1	64.5	0.27	99.4		1.38	1.11	1.11	1.58	5.13	0.67
	H-W4-2	62.4	0.27	101.3		1.41	0.98	1.02			
	H-W4-3	65.8	0.27	104.3		1.36	1.03	1.18			
UHSC FRP-wrapped	UH-W4-1*	108.0	0.35	117.4	103.0	0.96	0.81	0.88	1.09	2.74	0.52
	UH-W5-1	112.0	0.36	121.2	119.6	1.09	0.80	0.90	1.08	3.06	0.51
	UH-W6-1*	110.0	0.35	122.3		1.12	0.94	1.35	1.11	3.17	0.61

** indicates datasets that were included in a previous publication (Ozbakkaloglu and Akin [17]).*

*** indicates specimens that experienced problems either with loading or instrumentation.*

Table 3. Material properties of carbon fiber sheets

Fibre description	Properties reported by the manufacturer
Type	Carbon-High Tensile (MBrace CF 120)
Nominal thickness, t_f (mm)	0.117
Weight (g/m^2)	200
Elastic modulus, E_f (GPa)	240
Ultimate tensile stress, f_{fu} (MPa)	3800
Ultimate tensile strain, ε_{fu} (%)	1.55

Table 4. Average recorded strain reduction factors, k_ε

Concrete type	Confinement method	k_ε	S.D.	No.
All	All	0.623	0.118	52
	Tubes	0.598	0.129	32
	Wraps	0.664	0.085	20
NSC	All	0.747	0.099	11
	Tubes	0.759	0.152	5
	Wraps	0.737	0.028	6
HSC	All	0.651	0.074	22
	Tubes	0.647	0.078	11
	Wraps	0.656	0.073	11
UHSC	All	0.519	0.075	19
	Tubes	0.514	0.079	16
	Wraps	0.548	0.050	3

Table 5. Summary of models used to predict peak axial strength and ultimate axial strain of test specimens

Model	Peak Strength Expression	Ultimate Strain Expression
Benzaid et al. [29]	$\frac{f'_{cc}}{f'_{co}} = 1 + 2.2\frac{f_{lu,a}}{f'_{co}}$	$\frac{\varepsilon_{cu}}{\varepsilon_{co}} = 2 + 7.6\frac{f_{lu,a}}{f'_{co}}$
Bisby et al. [6]	$f'_{cc} = f'_{co} + 3.587\ f_{lu}^{\ 0.840}$	$\varepsilon_{cu} = \varepsilon_{co} + k_2\left(\frac{f_{lu}}{f'_{co}}\right)$ $k_2 = 0.0240$
Jiang and Teng [32]	$\frac{f'_{cc}}{f'_{co}} = 1 + 3.5\left(\frac{E_l}{(f'_{co}/\varepsilon_{co})} - 0.01\right)\left(\frac{\varepsilon_{h,rup}}{\varepsilon_{co}}\right)$	$\frac{\varepsilon_{cu}}{\varepsilon_{co}} = 1.65 + 6.5\left(\frac{E_l}{(f'_{co}/\varepsilon_{co})}\right)^{0.8}\left(\frac{\varepsilon_{h,rup}}{\varepsilon_{co}}\right)^{1.45}$
Lam and Teng [5]	$\frac{f'_{cc}}{f'_{co}} = 1 + 3.3\frac{f_{lu,a}}{f'_{co}}$	$\frac{\varepsilon_{cu}}{\varepsilon_{co}} = 1.75 + 5.53\left(\frac{f_{lu,a}}{f'_{co}}\right)\left(\frac{\varepsilon_{frp}}{\varepsilon_{co}}\right)^{0.45}$
Samaan et al. [33]	$f'_{cc} = f'_{co} + 6.0\left(f_{lu}\right)^{0.7}$	$\varepsilon_{cu} = \frac{f'_{cc} - f_o}{E_{c2}}$ $f_o = 0.872\ f'_{co} + 0.371\ f_{lu} + 6.258$ $E_{c2} = 245.61\ f'^{\ 0.2}_{co} + 1.3456\left(\frac{E_{frp}\ t_{frp}}{D}\right)$
Shehata et al. [34]	$\frac{f'_{cc}}{f'_{co}} = 1 + 2\frac{f_{lu}}{f'_{co}}$	$\frac{\varepsilon_{cu}}{\varepsilon_{co}} = 1 + 632\left(\frac{f_{lu}}{f'_{co}}\frac{f'_{cc}}{E_f}\right)^{0.5}$
Tamuzs et al. [30, 31]	$\frac{f'_{cc}}{f'_{co}} = 1 + 4.2\frac{f_{lu,a}}{f'_{co}}$	$\varepsilon_{cu} = \varepsilon_{co} + \frac{\varepsilon_{h,rup} - \nu_c\varepsilon_{co}}{\mu_{tu}}$ $\mu_{tu} = 5.9\left(\frac{E_l}{f'_{co}}\right)^{-0.65}$
Teng et al. [35]	Same as Jiang and Teng [32]	$\frac{\varepsilon_{cu}}{\varepsilon_{co}} = 1.75 + 6.5\left(\frac{E_l}{(f'_{co}/\varepsilon_{co})}\right)^{0.8}\left(\frac{\varepsilon_{h,rup}}{\varepsilon_{co}}\right)^{1.45}$
Wei and Wu [36]	$\frac{f'_{cc}}{f'_{co}} = 1 + 2.2\left(\frac{f_{lu}}{f'_{co}}\right)^{0.94}$	$\frac{\varepsilon_{cu}}{\varepsilon_{co}} = 1.75 + 12\left(\frac{f_{lu}}{f'_{co}}\right)^{0.75}\left(\frac{f_{30}}{f'_{co}}\right)^{0.62}$
Youssef et al. [37]	$\frac{f'_{cc}}{f'_{co}} = 1 + 2.25\left(\frac{f_{lu}}{f'_{co}}\right)^{\frac{5}{4}}$	$\varepsilon_{cu} = 0.003368 + 0.259\left(\frac{f_{lu}}{f'_{co}}\right)\left(\frac{f_{frp}}{E_{frp}}\right)^{\frac{1}{2}}$

Table 6. Statistics on model predictions of strength and strain enhancement ratios of test specimens

Model	Concrete Strength	Prediction of f'_{cc}/f'_{co}			Prediction of $\varepsilon_{cu}/\varepsilon_{co}$		
		MSE	AAE (%)	LTS	MSE	AAE (%)	LTS
Benzaid et al. [29]	NSC	0.01	5.8	0.96	6.22	35.6	0.58
	HSC	0.02	10.8	1.07	1.31	19.6	0.77
	UHSC	0.04	14.9	1.14	0.14	11.9	1.02
Bisby et al. [6]	NSC	0.03	12.3	1.10	3.84	28.6	0.67
	HSC	0.12	26.7	1.25	0.90	17.9	0.81
	UHSC	0.20	37.8	1.38	0.12	10.9	1.01
Jiang and Teng [32]	NSC	0.00	3.3	0.99	0.86	10.1	0.88
	HSC	0.04	15.5	1.14	0.61	18.1	1.08
	UHSC	0.09	23.7	1.23	1.24	39.6	1.34
Lam and Teng [5]	NSC	0.03	11.7	1.11	2.35	20.4	0.75
	HSC	0.10	24.8	1.23	0.47	10.7	0.91
	UHSC	0.13	29.4	1.29	0.24	17.4	1.12
Samaan et al. [33]	NSC	0.10	22.1	1.19	44.82	135.2	2.06
	HSC	0.17	32.7	1.30	49.57	175.1	2.53
	UHSC	0.22	40.1	1.40	41.81	236.1	2.96
Shehata et al. [34]	NSC	0.01	6.1	1.02	0.62	14.8	0.98
	HSC	0.08	21.2	1.19	11.76	80.9	1.75
	UHSC	0.19	36.0	1.36	45.99	225.5	3.17
Tamuzs et al. [30, 31]	NSC	0.12	22.9	1.23	1.36	21.7	1.15
	HSC	0.23	37.3	1.36	0.97	24.2	1.14
	UHSC	0.25	41.3	1.41	0.36	21.0	1.16
Teng et al. [35]	NSC	0.00	3.3	0.99	0.76	10.1	0.90
	HSC	0.04	15.5	1.14	0.70	20.0	1.10
	UHSC	0.09	23.7	1.23	1.46	43.2	1.37
Wei and Wu [36]	NSC	0.02	10.2	1.08	0.96	16.3	0.93
	HSC	0.14	29.2	1.27	0.43	13.4	1.06
	UHSC	0.30	45.1	1.45	1.13	38.7	1.30
Youssef et al. [37]	NSC	0.01	5.6	0.95	0.54	11.3	0.95
	HSC	0.04	13.6	1.12	0.49	12.7	1.07
	UHSC	0.12	27.8	1.28	0.83	30.1	1.25

LIST OF FIGURES

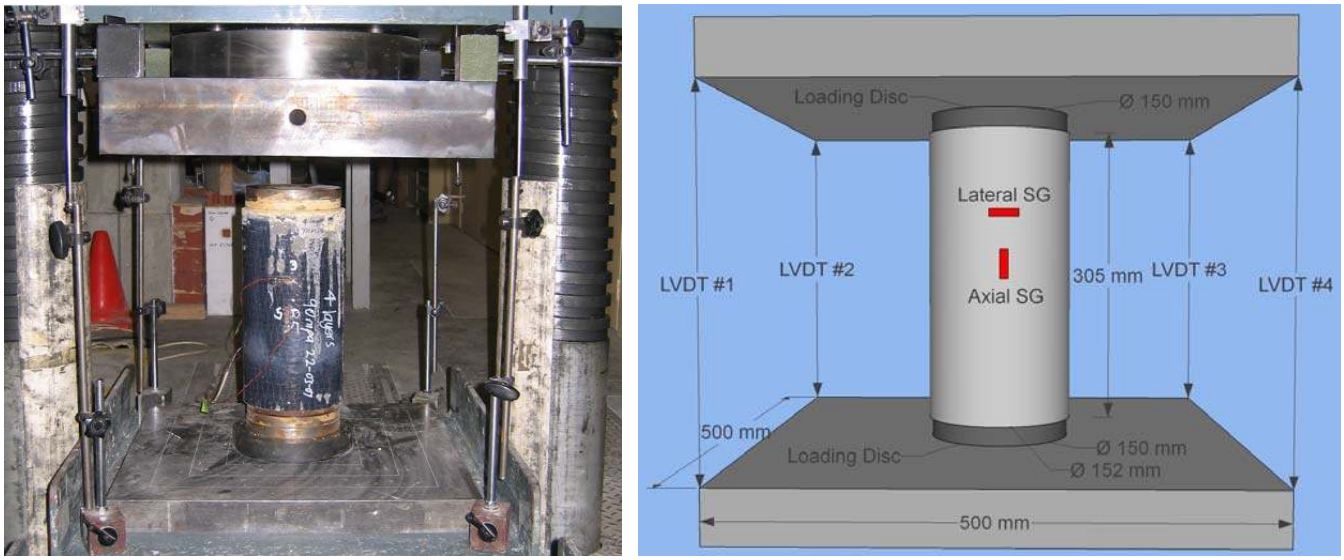

(a) *(b)*

Figure 1. Setup and instrumentation: a) specimen before testing; b) technical illustration

a) *b)* *c)*

Figure 2. Typical failure modes of test specimens: a) continuous shell rupture from top to bottom;

b) ringed rupture; c) top half rupture

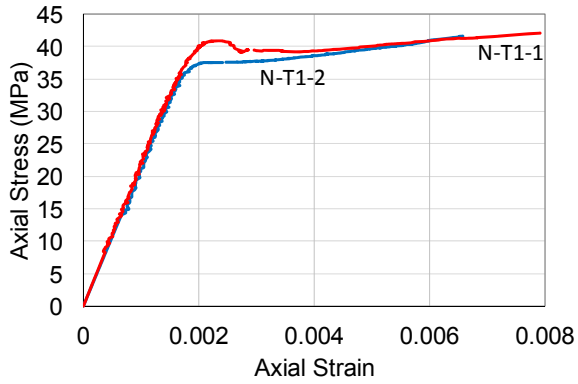
Axial Stress (MPa)
Axial Strain
N-T1-1
N-T1-2

a)

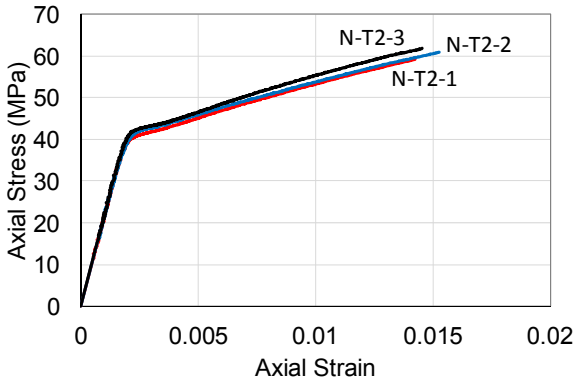
Axial Stress (MPa)
Axial Strain
N-T2-3
N-T2-2
N-T2-1

b)

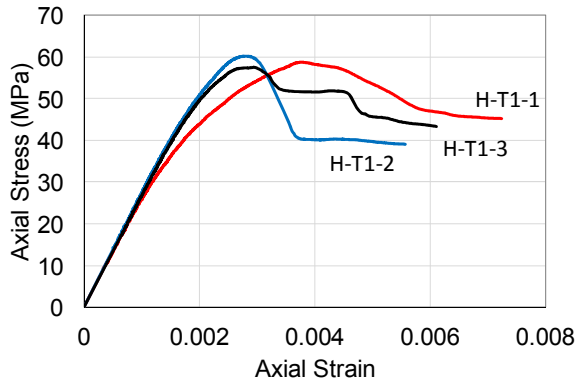
Axial Stress (MPa)
Axial Strain
H-T1-1
H-T1-3
H-T1-2

c)

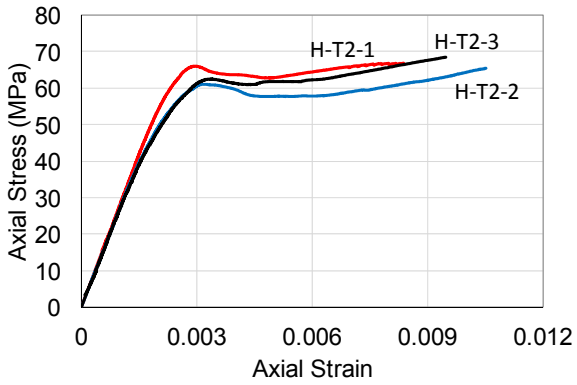
Axial Stress (MPa)
Axial Strain
H-T2-1
H-T2-3
H-T2-2

d)

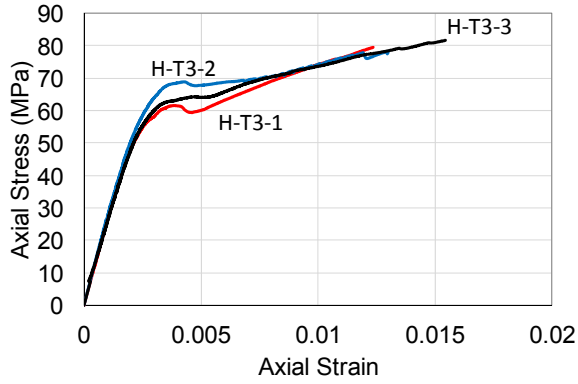
Axial Stress (MPa)
Axial Strain
H-T3-3
H-T3-2
H-T3-1

e)

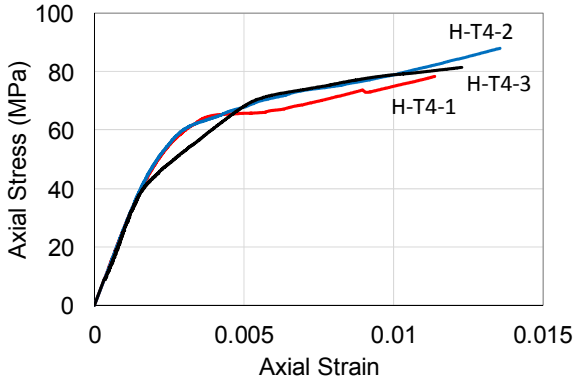
Axial Stress (MPa)
Axial Strain
H-T4-2
H-T4-3
H-T4-1

f)

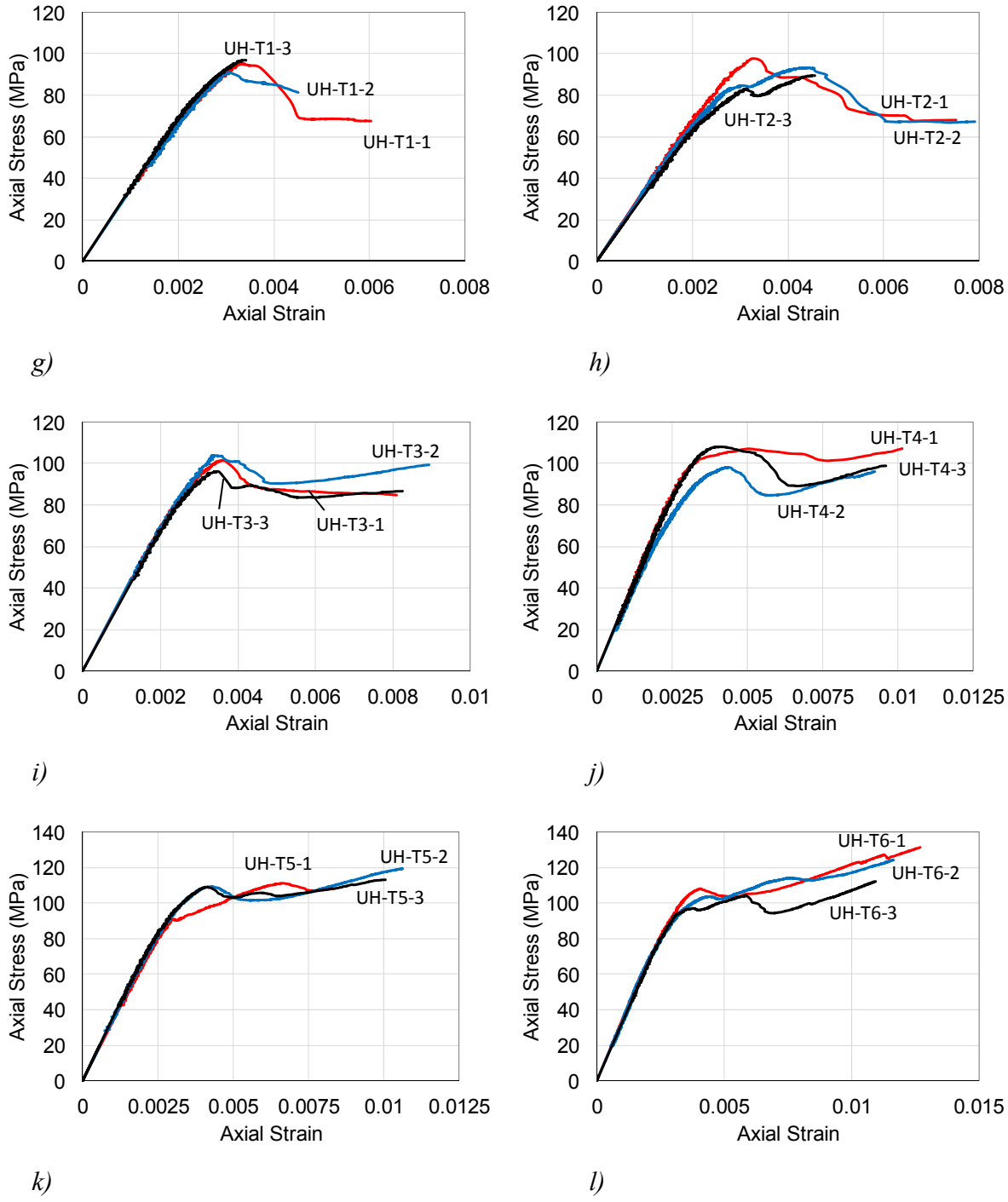

Figure 3. Axial stress-strain response of FRP tube-encased specimens: a) NSC, 1-layer; b) NSC, 2-layer; c) HSC, 1-layer; d) HSC, 2-layer; e) HSC, 3-layer; f) HSC, 4-layer; g) UHSC, 1-layer; h) UHSC, 2-layer; i) UHSC, 3-layer; j) UHSC, 4-layer; k) UHSC, 5-layer; l) UHSC, 6-layer

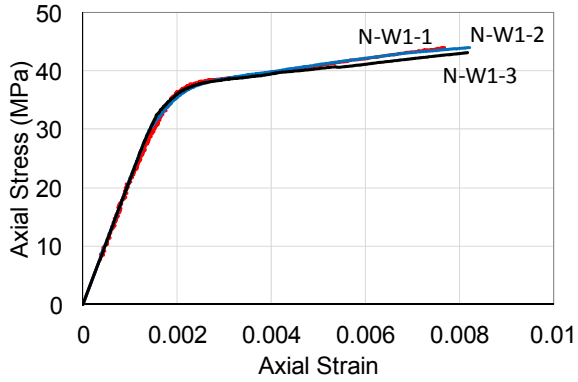
N-W1-1
N-W1-2
N-W1-3
Axial Stress (MPa)
Axial Strain
0
10
20
30
40
50
0
0.002
0.004
0.006
0.008
0.01

a)

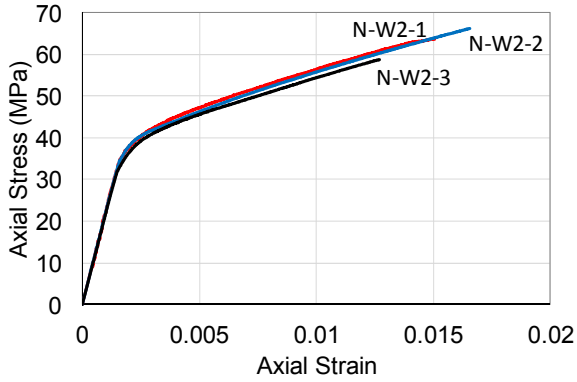
N-W2-1
N-W2-2
N-W2-3
Axial Stress (MPa)
Axial Strain
0
10
20
30
40
50
60
70
0
0.005
0.01
0.015
0.02

b)

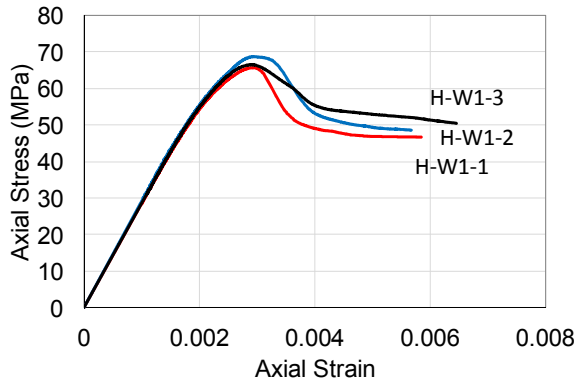
H-W1-3
H-W1-2
H-W1-1
Axial Stress (MPa)
Axial Strain
0
10
20
30
40
50
60
70
80
0
0.002
0.004
0.006
0.008

c)

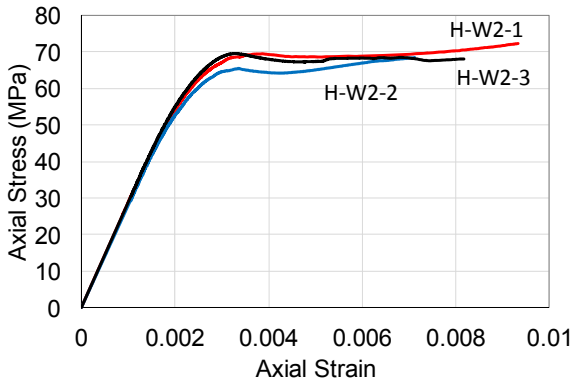
H-W2-1
H-W2-3
H-W2-2
Axial Stress (MPa)
Axial Strain
0
10
20
30
40
50
60
70
80
0
0.002
0.004
0.006
0.008
0.01

d)

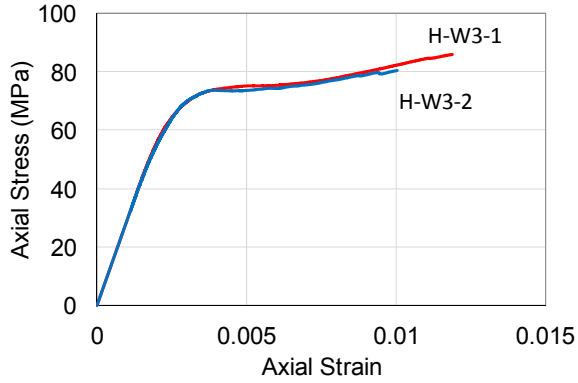
H-W3-1
H-W3-2
Axial Stress (MPa)
Axial Strain
0
20
40
60
80
100
0
0.005
0.01
0.015

e)

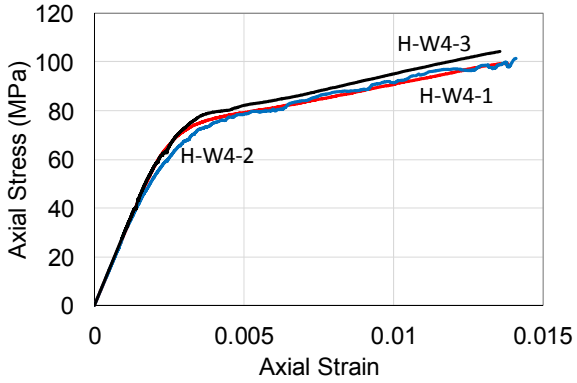
H-W4-3
H-W4-1
H-W4-2
Axial Stress (MPa)
Axial Strain
0
20
40
60
80
100
120
0
0.005
0.01
0.015

f)

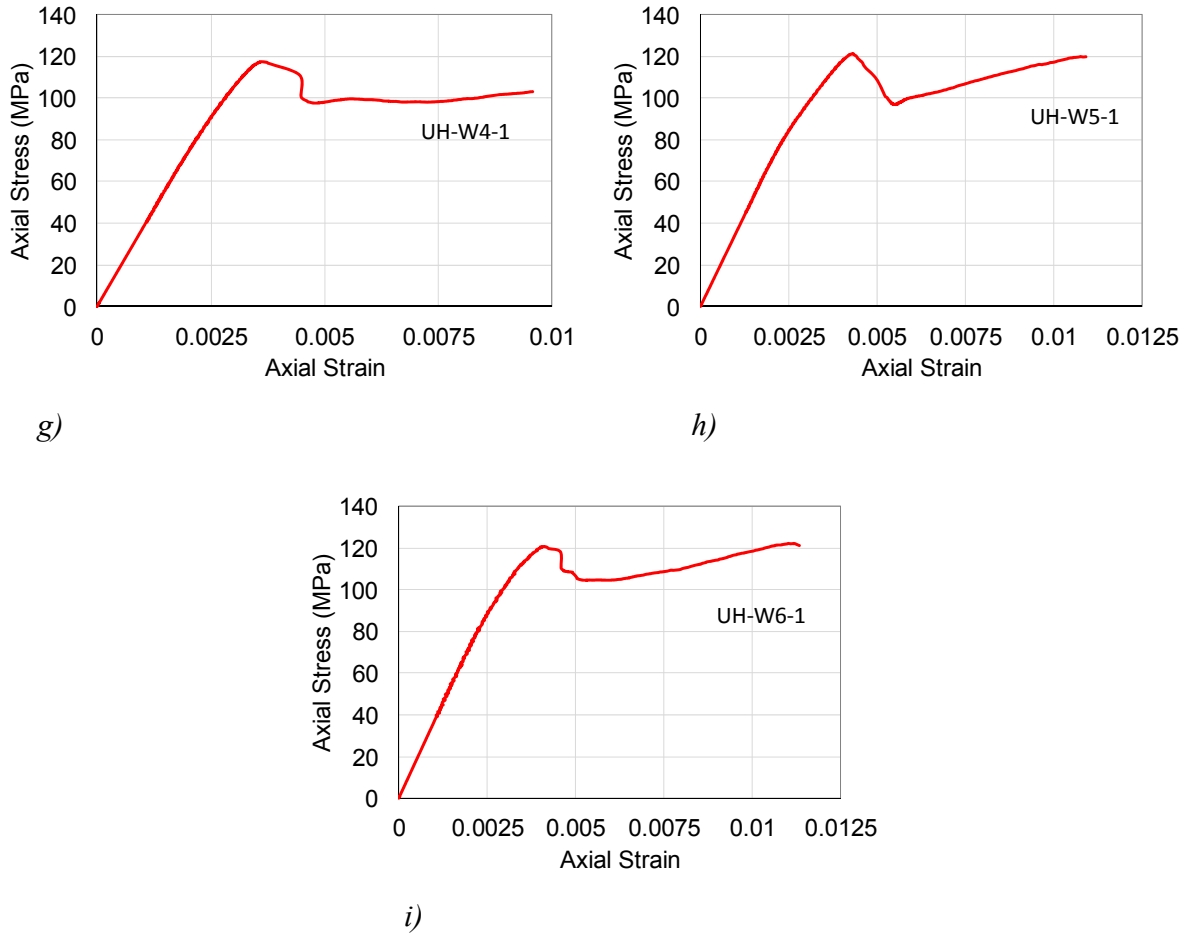

g) *h)*

i)

Figure 4. Axial stress-strain response of FRP-wrapped specimens: a) NSC, 1-layer; b) NSC, 2-layer; c) HSC, 1-layer; d) HSC, 2-layer; e) HSC, 3-layer; f) HSC, 4-layer; g) UHSC, 4-layer; h) UHSC, 5-layer; i) UHSC, 6-layer

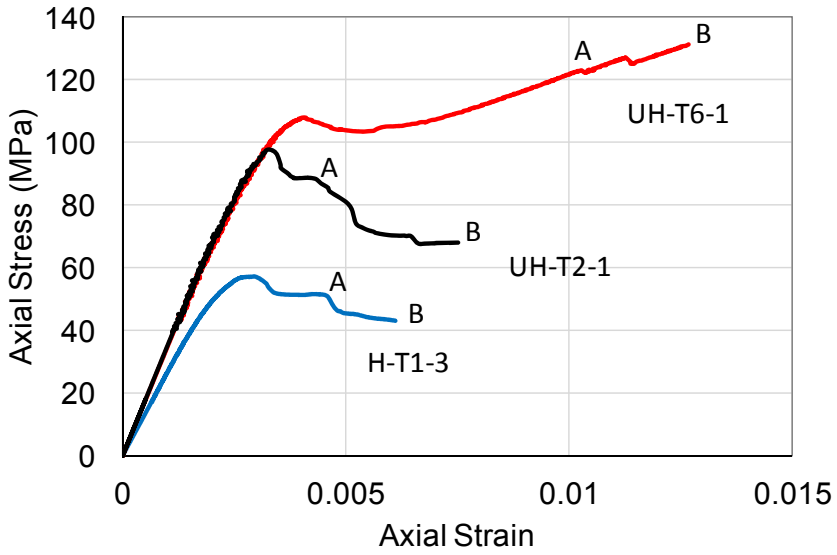

Figure 5. Definition of ultimate condition

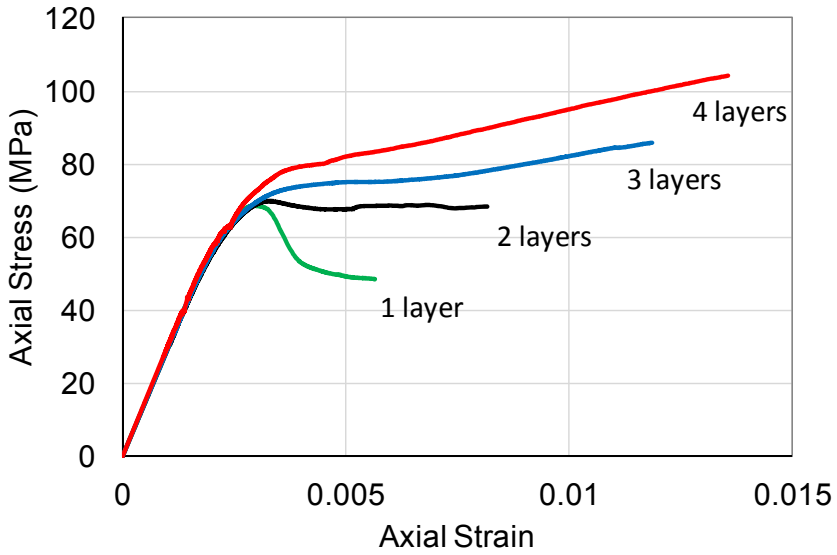

Figure 6. Influence of amount of confinement on FRP-wrapped HSC

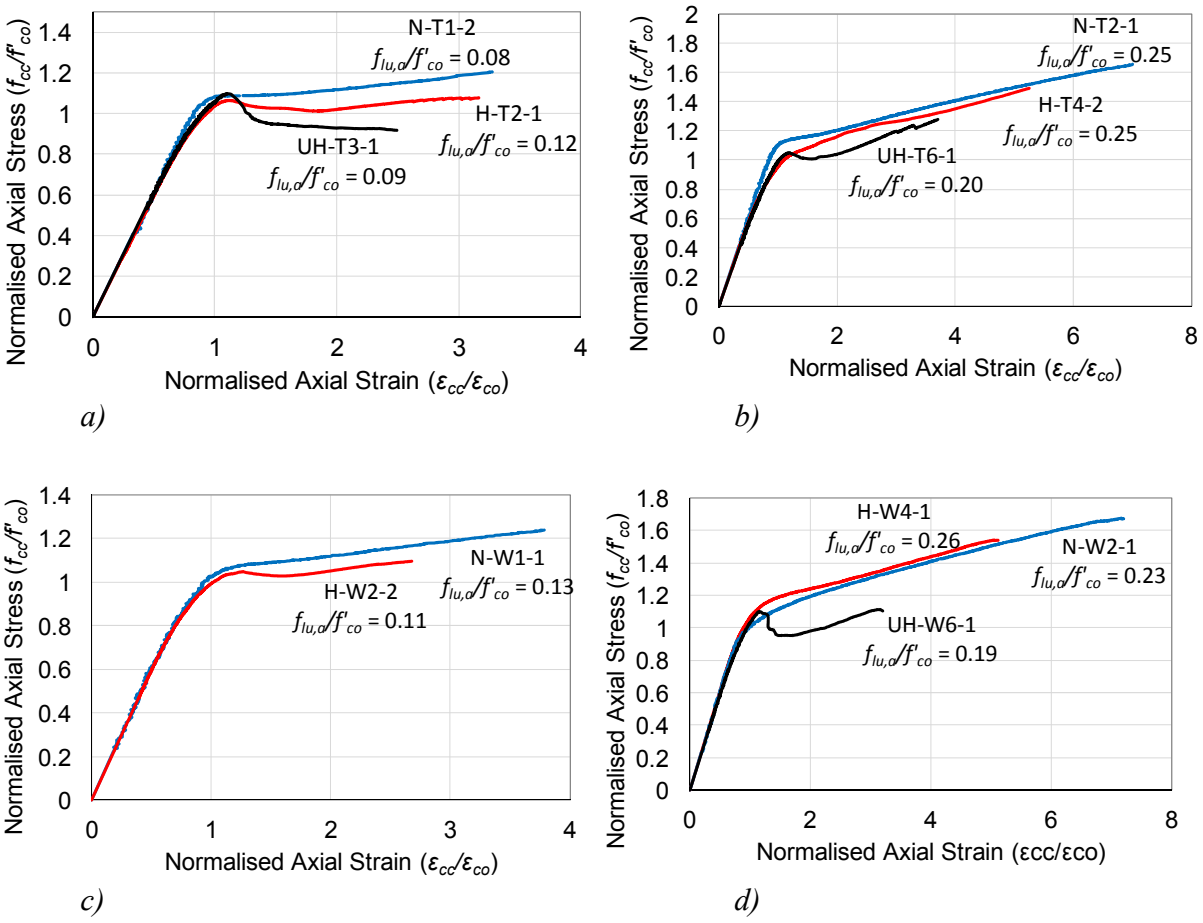

Figure 7. Influence of concrete strength on stress-strain behavior of test specimens:

a) FRP tube-encased, Group 1; b) FRP tube-encased, Group 2; c) FRP-wrapped, Group 1; d) FRP-wrapped, Group 2

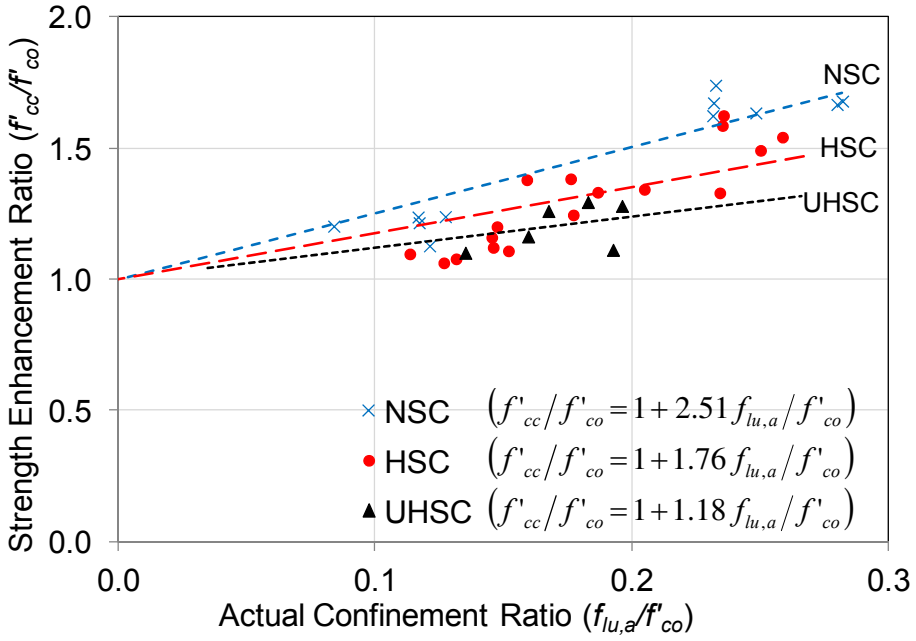

a)

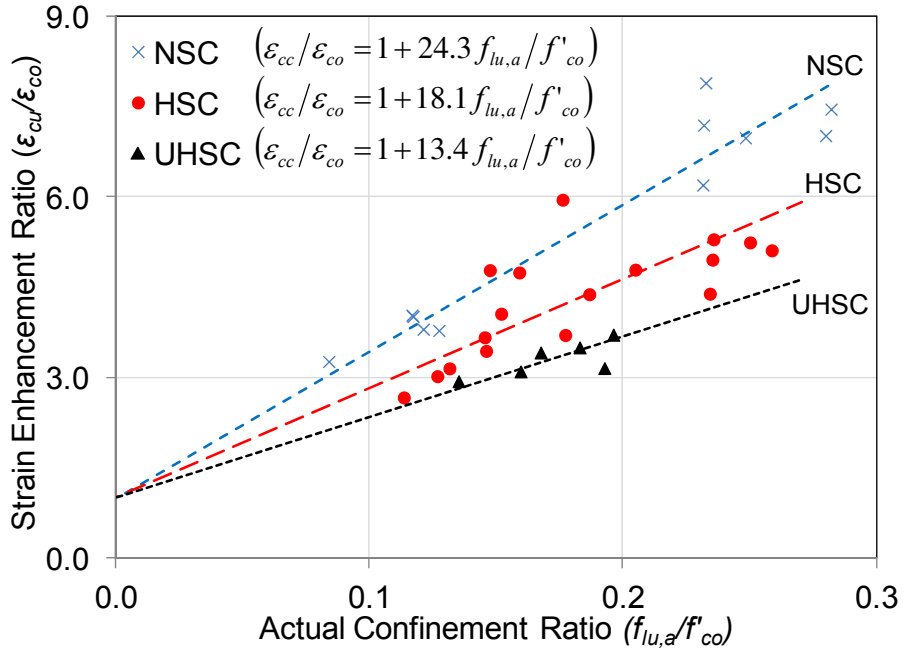

b)

Figure 8. Influence of concrete strength on strength and strain enhancement ratios of test specimens: a) strength enhancement ratio; b) strain enhancement ratio

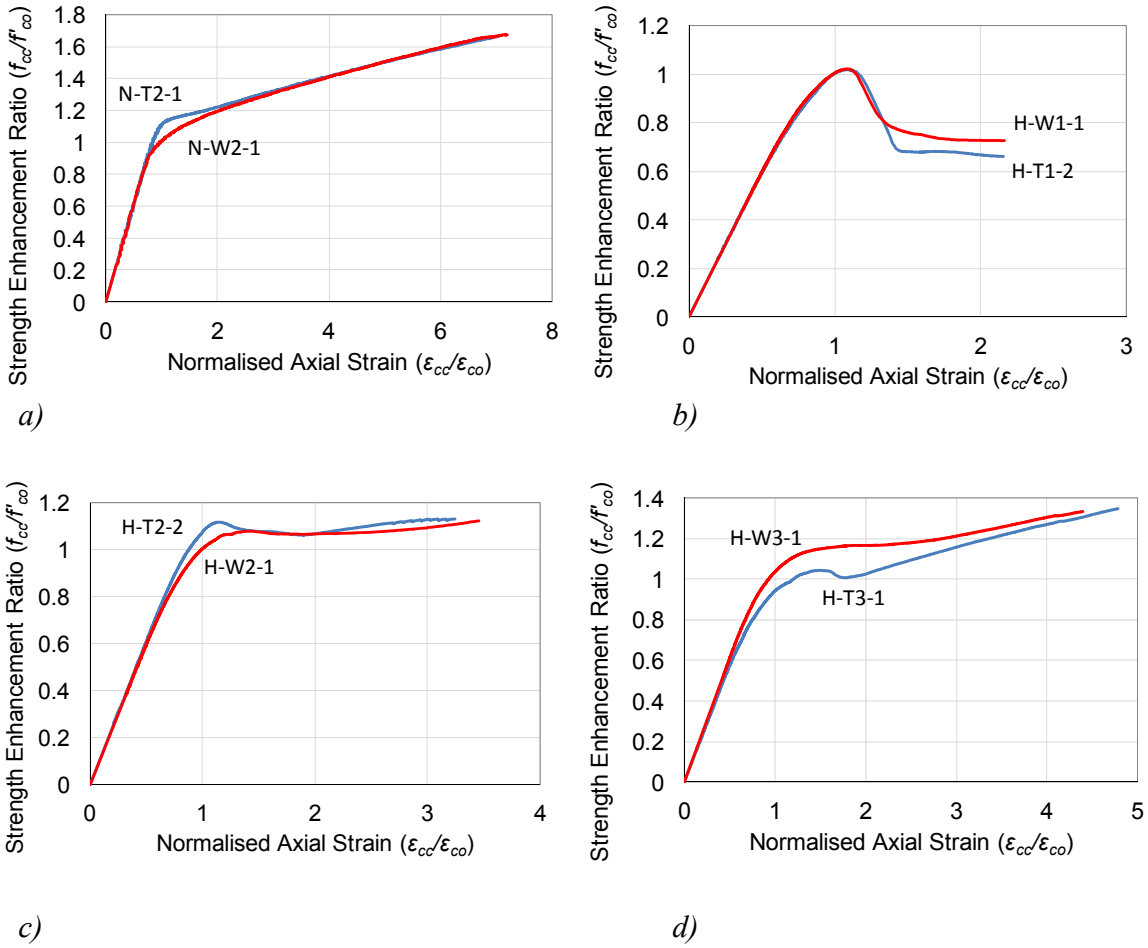

Figure 9. Influence of confinement method on the transition region of stress-strain curves: a) NSC, 2-layer FRP; b) HSC, 1-layer FRP; c) HSC, 2-layer FRP; d) HSC, 3-layer FRP

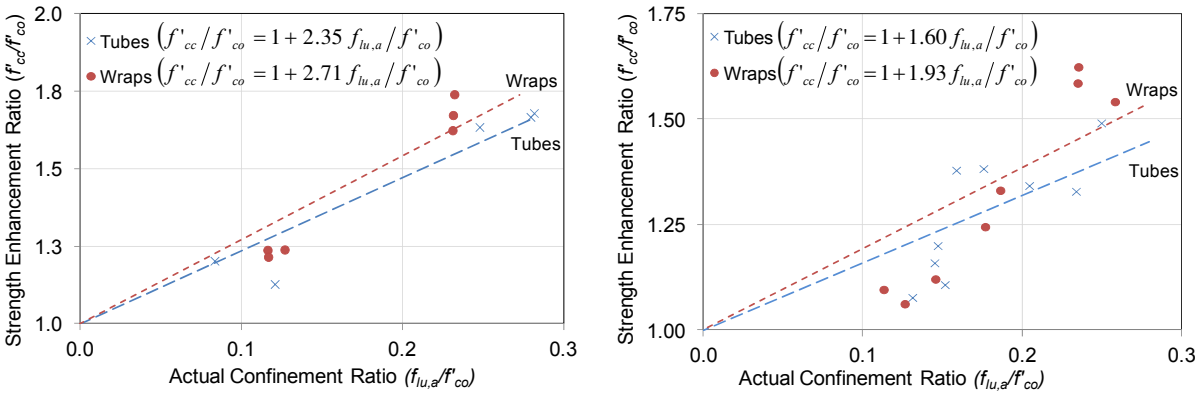

a) *b)*

Figure 10. Influence of confinement method on strength enhancement ratios of test specimens: a) NSC specimens; b) HSC specimens

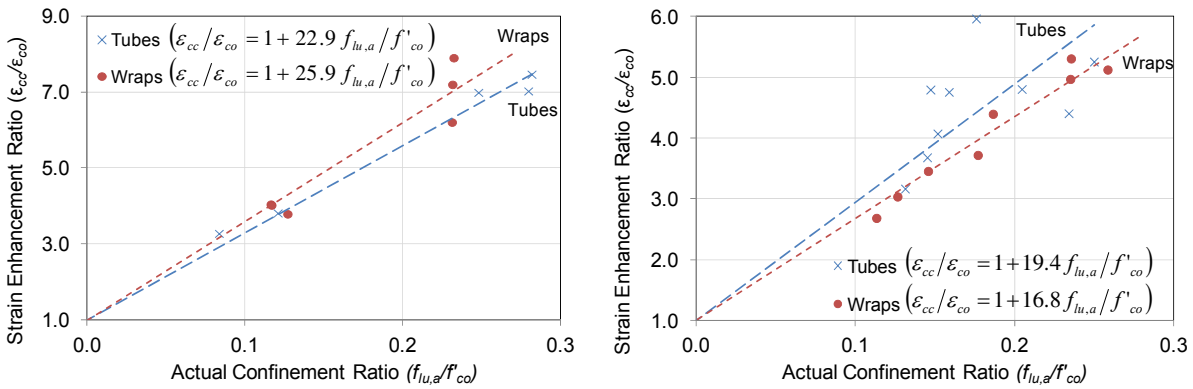

a) *b)*

Figure 11. Influence of confinement method on strain enhancement ratio of test specimens: a) NSC specimens; b) HSC specimens

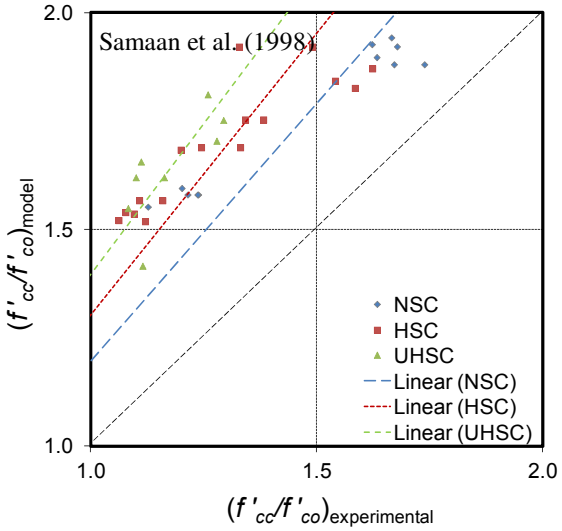
Samaan et al. (1998)
NSC
HSC
UHSC
Linear (NSC)
Linear (HSC)
Linear (UHSC)
2.0
1.5
1.0
1.0
1.5
2.0
$(f'_{cc}/f'_{co})_{model}$
$(f'_{cc}/f'_{co})_{experimental}$

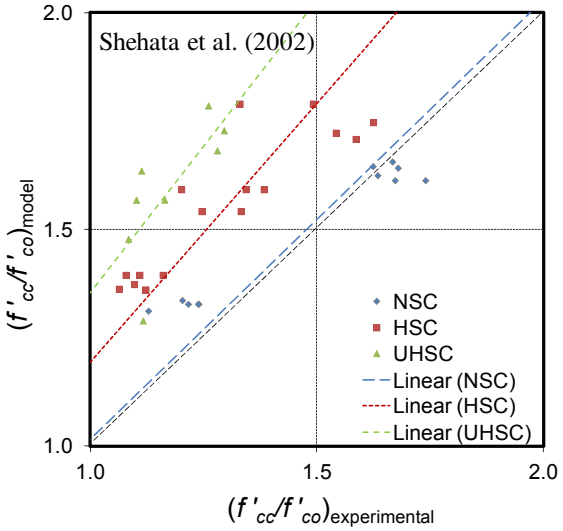
Shehata et al. (2002)
NSC
HSC
UHSC
Linear (NSC)
Linear (HSC)
Linear (UHSC)
2.0
1.5
1.0
1.0
1.5
2.0
$(f'_{cc}/f'_{co})_{model}$
$(f'_{cc}/f'_{co})_{experimental}$

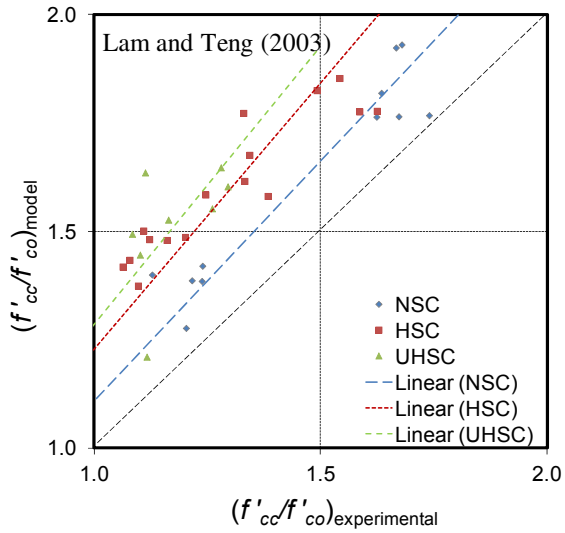
Lam and Teng (2003)
NSC
HSC
UHSC
Linear (NSC)
Linear (HSC)
Linear (UHSC)
2.0
1.5
1.0
1.0
1.5
2.0
$(f'_{cc}/f'_{co})_{model}$
$(f'_{cc}/f'_{co})_{experimental}$

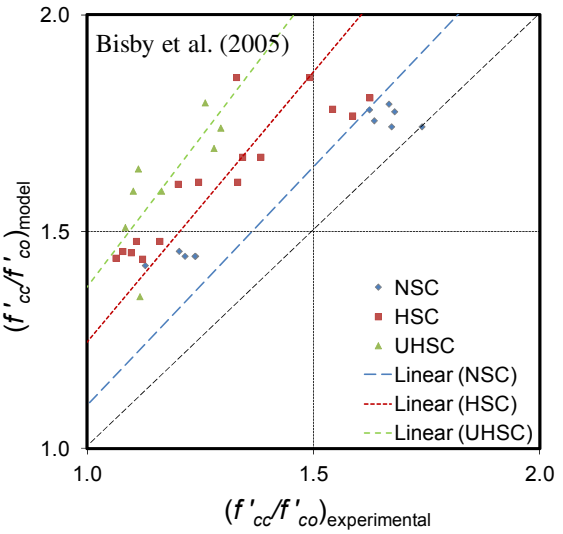
Bisby et al. (2005)
NSC
HSC
UHSC
Linear (NSC)
Linear (HSC)
Linear (UHSC)
2.0
1.5
1.0
1.0
1.5
2.0
$(f'_{cc}/f'_{co})_{model}$
$(f'_{cc}/f'_{co})_{experimental}$

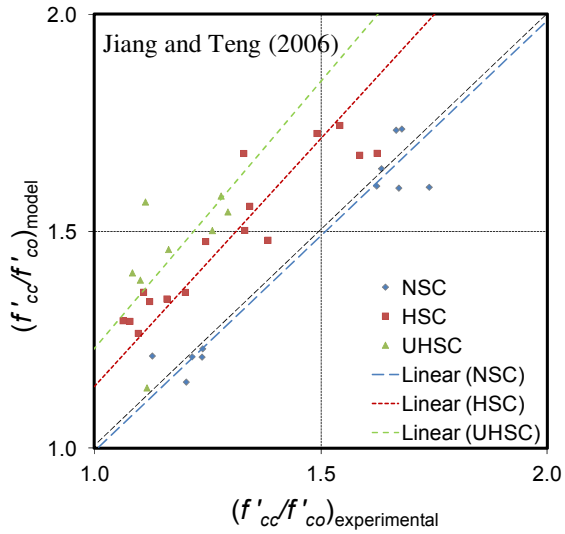
Jiang and Teng (2006)
NSC
HSC
UHSC
Linear (NSC)
Linear (HSC)
Linear (UHSC)
2.0
1.5
1.0
1.0
1.5
2.0
$(f'_{cc}/f'_{co})_{model}$
$(f'_{cc}/f'_{co})_{experimental}$

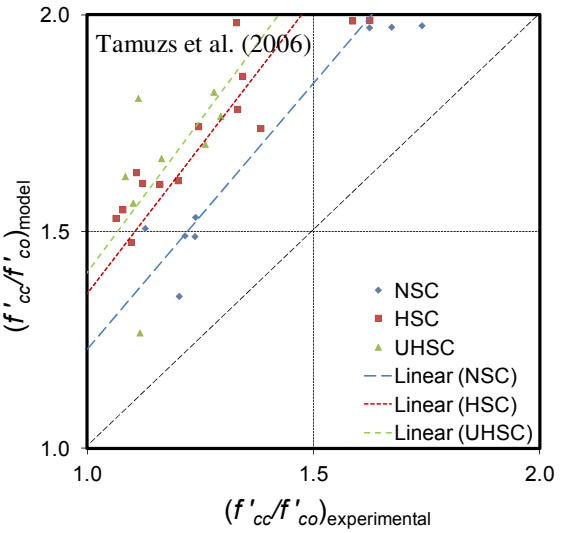
Tamuzs et al. (2006)
NSC
HSC
UHSC
Linear (NSC)
Linear (HSC)
Linear (UHSC)
2.0
1.5
1.0
1.0
1.5
2.0
$(f'_{cc}/f'_{co})_{model}$
$(f'_{cc}/f'_{co})_{experimental}$

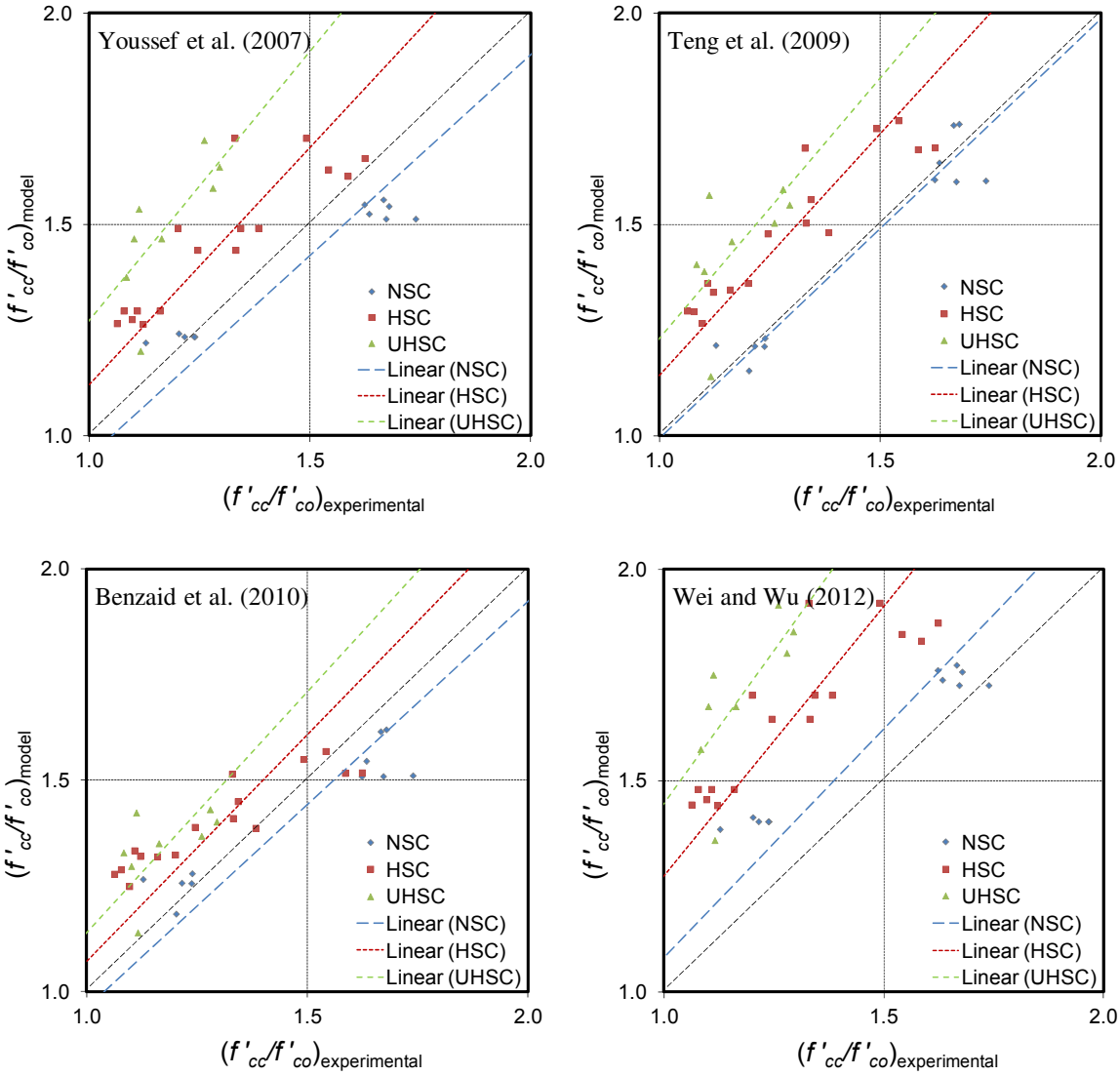

Figure 12. Performance of models in predicting strength enhancement ratio

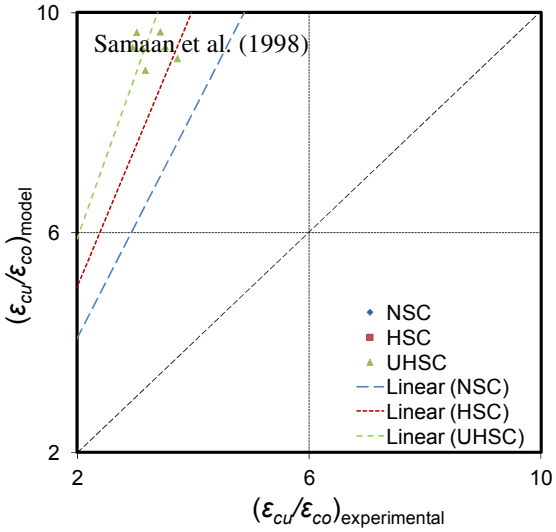
Samaan et al. (1998)
NSC
HSC
UHSC
Linear (NSC)
Linear (HSC)
Linear (UHSC)
$(\varepsilon_{cu}/\varepsilon_{co})_{model}$
$(\varepsilon_{cu}/\varepsilon_{co})_{experimental}$
2
6
10

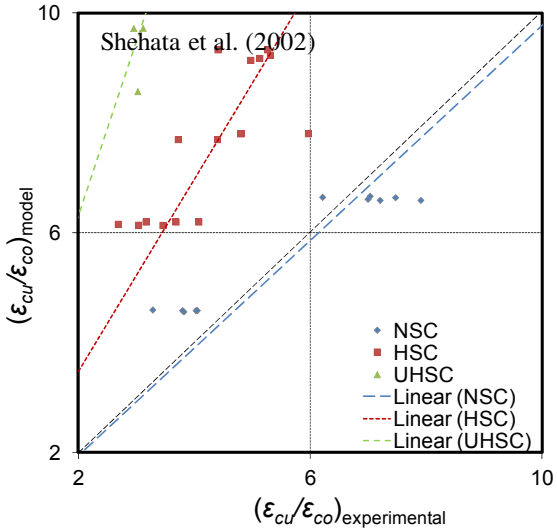
Shehata et al. (2002)
NSC
HSC
UHSC
Linear (NSC)
Linear (HSC)
Linear (UHSC)
$(\varepsilon_{cu}/\varepsilon_{co})_{model}$
$(\varepsilon_{cu}/\varepsilon_{co})_{experimental}$
2
6
10

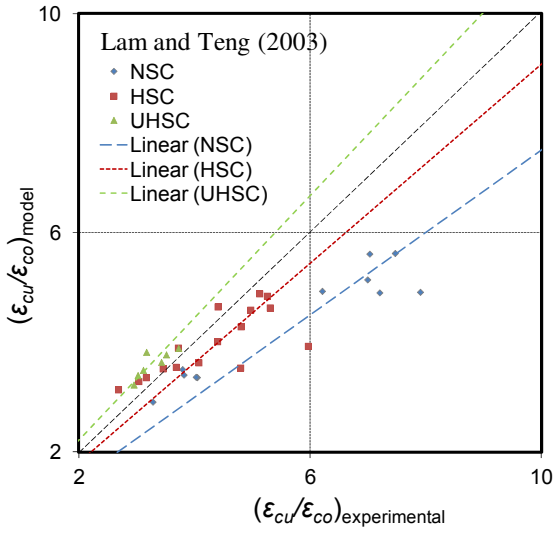
Lam and Teng (2003)
NSC
HSC
UHSC
Linear (NSC)
Linear (HSC)
Linear (UHSC)
$(\varepsilon_{cu}/\varepsilon_{co})_{model}$
$(\varepsilon_{cu}/\varepsilon_{co})_{experimental}$
2
6
10

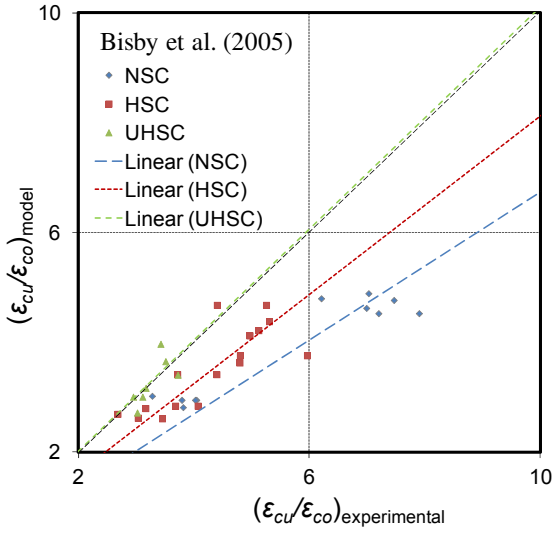
Bisby et al. (2005)
NSC
HSC
UHSC
Linear (NSC)
Linear (HSC)
Linear (UHSC)
$(\varepsilon_{cu}/\varepsilon_{co})_{model}$
$(\varepsilon_{cu}/\varepsilon_{co})_{experimental}$
2
6
10

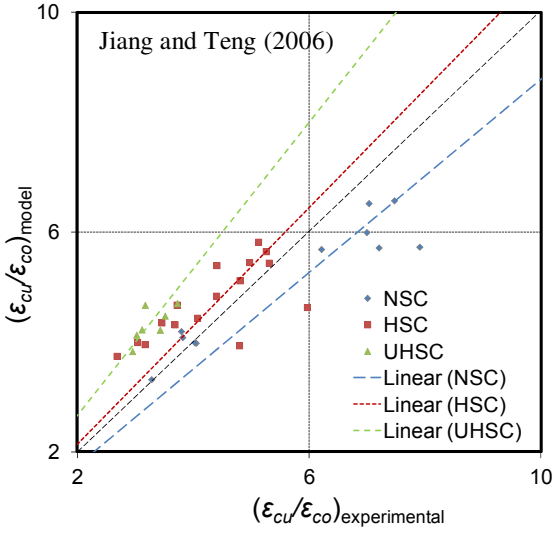
Jiang and Teng (2006)
NSC
HSC
UHSC
Linear (NSC)
Linear (HSC)
Linear (UHSC)
$(\varepsilon_{cu}/\varepsilon_{co})_{model}$
$(\varepsilon_{cu}/\varepsilon_{co})_{experimental}$
2
6
10

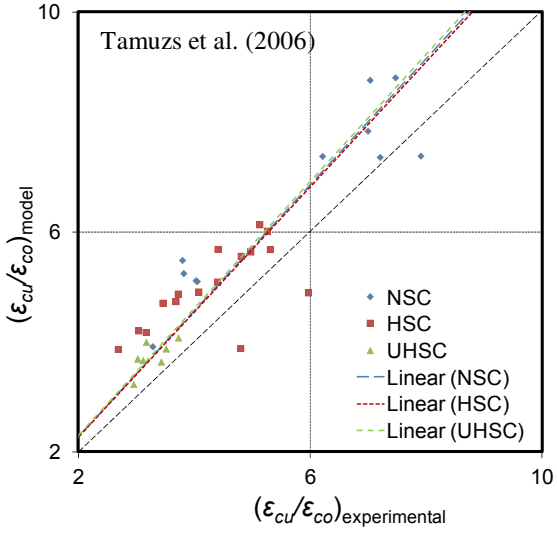
Tamuzs et al. (2006)
NSC
HSC
UHSC
Linear (NSC)
Linear (HSC)
Linear (UHSC)
$(\varepsilon_{cu}/\varepsilon_{co})_{model}$
$(\varepsilon_{cu}/\varepsilon_{co})_{experimental}$
2
6
10

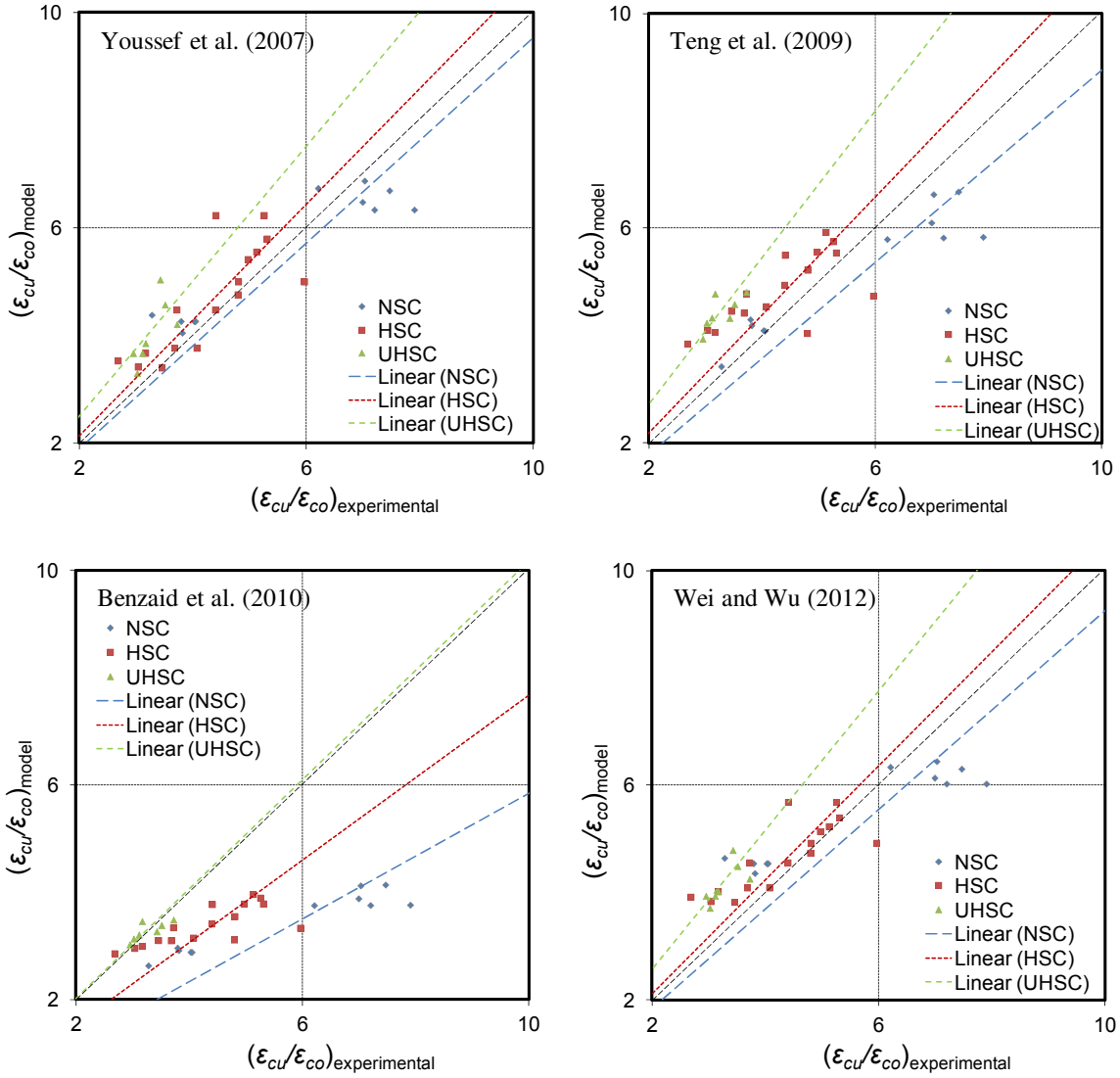

Figure 13. Performance of models in predicting strain enhancement ratio